doi:10.1038/nature25979

Extensive impact of non-antibiotic drugs on human gut bacteria

Lisa Maier[1]*, Mihaela Pruteanu[1]†*, Michael Kuhn[2]*, Georg Zeller[2], Anja Telzerow[1], Exene Erin Anderson[1], Ana Rita Brochado[1], Keith Conrad Fernandez[1], Hitomi Dose[3], Hirotada Mori[3], Kiran Raosaheb Patil[2], Peer Bork[2,4,5,6] & Athanasios Typas[1,2]

A few commonly used non-antibiotic drugs have recently been associated with changes in gut microbiome composition, but the extent of this phenomenon is unknown. Here, we screened more than 1,000 marketed drugs against 40 representative gut bacterial strains, and found that 24% of the drugs with human targets, including members of all therapeutic classes, inhibited the growth of at least one strain *in vitro*. Particular classes, such as the chemically diverse antipsychotics, were overrepresented in this group. The effects of human-targeted drugs on gut bacteria are reflected on their antibiotic-like side effects in humans and are concordant with existing human cohort studies. Susceptibility to antibiotics and human-targeted drugs correlates across bacterial species, suggesting common resistance mechanisms, which we verified for some drugs. The potential risk of non-antibiotics promoting antibiotic resistance warrants further exploration. Our results provide a resource for future research on drug-microbiome interactions, opening new paths for side effect control and drug repurposing, and broadening our view of antibiotic resistance.

Pharmaceutical agents have both beneficial and undesirable effects. Studies on the mechanisms of action and off-target spectra of various drugs aim to improve their efficacy and reduce their side effects. Although many drugs have gastrointestinal side effects and the gut microbiome itself is pivotal for human health[1], the role of the gut microbiota in these processes is rarely considered. Recently, consumption of drugs designed to target human cells and not microbes, such as antidiabetics (metformin[2]), proton pump inhibitors (PPIs)[3,4], nonsteroidal anti-inflammatory drugs[5] and atypical antipsychotics (AAPs)[6], has been associated with changes in microbiome composition. A larger cohort study suggested that medication can alter gut microbiome composition more generally[7]. As it is unclear whether such effects are direct and go beyond the few drug classes studied, we systematically profiled interactions between drugs and individual gut bacteria. We aimed to generate a comprehensive resource of drug actions on the microbiome, which could facilitate more in-depth clinical and mechanistic studies, ultimately improving therapy and drug design.

A high-throughput drug screen on gut bacteria

To systematically map interactions between drugs and human gut bacteria, we monitored the growth of 40 representative isolates upon treatment with 1,197 compounds in modified Gifu anaerobic medium (mGAM) broth, which partially recapitulates the species relative abundances in human gut microbiomes[8], under anaerobic conditions at 37 °C (Extended Data Fig. 1a). We used the Prestwick Chemical Library, which consists mostly of off-patent Federal Drug Administration (FDA)-approved compounds with high chemical and pharmacological diversity. Most compounds are administered to humans (1,079), and they cover all main therapeutic classes (Supplementary Table 1). Three quarters (835) of the compounds are human-targeted drugs (that is, have molecular targets in human cells), whereas the rest are anti-infectives: 156 with antibacterial activity (144 antibiotics, 12 antiseptics) and 88 effective against fungi, viruses or parasites (Fig. 1a). All compounds were screened at 20 μM, which is within the range of what is commonly used in high-throughput drug screens[9].

For our screen to be representative of the gut microbiome of healthy individuals, we selected a set of ubiquitous gut bacterial species (Supplementary Table 2). Prevalence and abundance in the human gut, and phylogenetic diversity, were our main selection criteria (Extended Data Fig. 1b), although we were occasionally constrained by strain unavailability or irreproducible growth in mGAM. In total, we included 40 human gut isolates from 38 bacterial species and 21 genera (*Escherichia coli* and *Bacteroides fragilis* were represented by two strains each), accounting together for 78% of the median assignable relative abundance of the human gut microbiome at genus level (60% at species level; Extended Data Fig. 1c). Most strains were commensals, covering 31 of 60 sequenced species detected at a relative abundance of 1% or more and prevalence of at least 50% in fecal samples from asymptomatic humans from three continents (Extended Data Fig. 1d). In addition, the set included four pathobionts (*Clostridium difficile*, *Clostridium perfringens*, *Fusobacterium nucleatum* and an enterotoxigenic strain of *B. fragilis*), a probiotic (*Lactobacillus paracasei*) and two commensal *Clostridia* species (*C. ramosum* and *C. saccharolyticum*). All 38 species are found in the gut of healthy individuals and are part of a larger strain resource panel for the healthy human gut microbiome[8].

We screened all compounds in multiwell plates, measuring optical density over time to monitor growth, and quantifying the area under the growth curve (AUC) up to the time point at which controls with unperturbed growth transitioned to stationary phase (see Methods; Extended Data Fig. 2). We obtained at least three biological replicates per strain, and these replicates correlated highly (Extended Data Fig. 2c). We then tested for significant deviations from the normalized AUC distribution of samples with unperturbed growth, combining *P* values across replicates and correcting for multiple hypothesis testing on the complete matrix of compounds and strains (see Methods; Extended Data Fig. 2). Drugs that significantly reduced the growth of

[1]European Molecular Biology Laboratory, Genome Biology Unit, 69117 Heidelberg, Germany. [2]European Molecular Biology Laboratory, Structural and Computational Biology Unit, 69117 Heidelberg, Germany. [3]Graduate School of Biological Sciences, Nara Institute of Science and Technology, 630-0101 Ikoma, Japan. [4]Max-Delbrück-Centre for Molecular Medicine, 13125 Berlin, Germany. [5]Molecular Medicine Partnership Unit, 69120 Heidelberg, Germany. [6]Department of Bioinformatics, Biocenter, University of Würzburg, 97024 Würzburg, Germany. †Present address: Institute for Biology, Humboldt University Berlin, 10115 Berlin, Germany.
*These authors contributed equally to this work.

© 2018 Macmillan Publishers Limited, part of Springer Nature. All rights reserved.

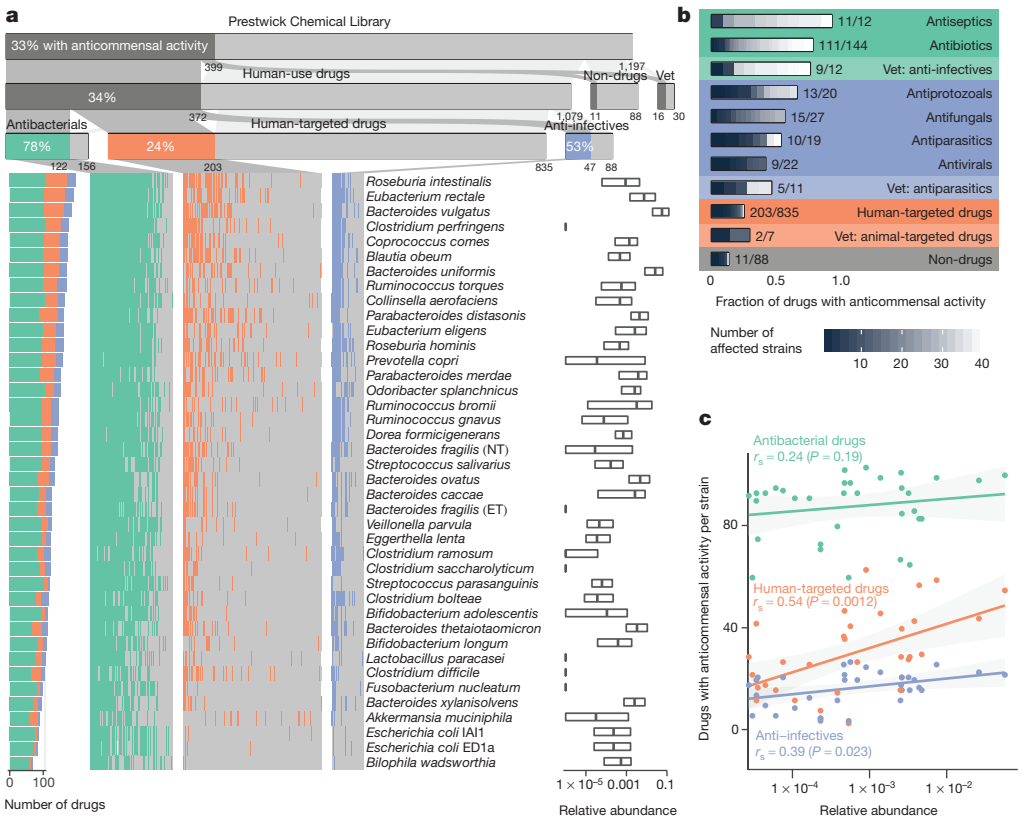

Figure 1 | Systematic profiling of marketed drugs on a representative panel of human gut microbial species. a, Broad impact of pharmaceuticals on the human gut microbiota. Compounds from the Prestwick Chemical Library are divided into drugs used in humans, drugs used exclusively in animals (vet) and compounds without medical or veterinary use (non-drugs). Human-use drugs are further categorized according to targeted organism. Strain–drug pairs (that is, instances in which a drug significantly reduced the growth of a specific strain; see Methods) are highlighted with a vertical coloured bar in the matrix. Bacterial strains are sorted by drug sensitivity. The relative abundances of each strain in four cohort studies of healthy individuals are displayed on the right (boxes correspond to interquartile range (IQR) and central line to median relative abundance). **b**, Fractions of drugs with anticommensal activity by sub-category. Grey scale within bars denotes inhibition spectrum (the number of affected strains per drug). **c**, Correlation between species abundance in the human microbiome and drug sensitivity. For each strain ($n = 40$), the number of drugs that affect its growth is plotted against its median relative abundance in the human gut microbiome. Lines depict the best linear fit, r_S the Spearman correlation and grey shading the 95% confidence interval of the linear fit. All drugs, and in particular human-targeted drugs, inhibit the growth of more abundant species more than that of less abundant species.

at least one strain (false discovery rate (FDR) < 0.01), were classified as hits with anticommensal activity (Supplementary Table 3a), reflecting their potential to modulate the human gut microbiota.

Of the 156 antibacterials tested, 78% were active against at least one species, typically with a broad activity spectrum (Fig. 1a, b). Inactive antibiotics belong mainly to the sulfonamides (which are inactive in our medium according to the manufacturer's guidelines), aminoglycosides (which have compromised activity under anaerobic conditions[10]) and specific antimycobacterial drugs. Antibiotics are used to inhibit pathogens, but as expected, also target gut commensals. The medical importance of this collateral damage to the resident microbiome has recently been becoming clearer[11]. Nevertheless, to our knowledge, drug–microbiome species relationships have not previously been mapped at this scale.

Notably, 27% of the non-antibiotic drugs were also active in our screen. More than half of the anti-infectives against viruses or eukaryotes exhibited anticommensal activity (47 drugs; Fig. 1a, b). Antibacterial activity has been previously reported for many of these drugs, including the antifungal imidazoles[12] (11 in our screen), but not for others (for example, the antivirals saquinavir and trifluridine). More noteworthy is the anticommensal activity of 203 (24%) of the human-targeted drugs. Most were effective against only a few strains, with the exception of 40 drugs that affected at least 10 strains. Fourteen of these had, to our knowledge, not been previously reported to have direct antibacterial activity (Supplementary Table 3b). Among known human-targeted drugs with anticommensal activity, auranofin has recently been reported to have broad-spectrum bactericidal activity[13], and the ovulation stimulant clomiphene inhibits a conserved bacterial enzyme in the synthesis of an essential precursor for cell wall carbohydrate polymers[14]. Such drugs or their scaffolds can be used for repurposing towards broad-spectrum antibiotics, especially as many have minimal inhibitory concentrations (MICs) in the sub-microgram per millilitre range (Supplementary Table 4). By contrast, the microbial narrow-spectrum specificity of most human-targeted drugs could aid the development of microbiome modulators.

Bacterial species showed varied responses to drugs, with the abundant *Roseburia intestinalis*, *Eubacterium rectale* and *Bacteroides vulgatus* being the most sensitive, and γ-proteobacteria representatives being the most resistant (Fig. 1a). Overall, species with higher relative abundance across healthy individuals were significantly more susceptible to human-targeted drugs ($P = 0.0012$ based on Spearman correlation; Fig. 1c). This suggests that human-targeted drugs have an even larger impact on the gut microbiome, with key species related to healthy status[15], such as major butyrate producers (*E. rectale*, *R. intestinalis*, *Coprococcus comes*) and propionate producers (*B. vulgatus*, *Prevotella copri*, *Blautia obeum*)[16], and enterotype drivers (*P. copri*)[17], being relatively more affected.

Dose relevance and validation of the drug screen

We sought to address how close the screening concentration (20 μM) was to drug concentrations in the terminal ileum and colon, where most gut microbes reside[18]. However, drug concentrations are

© 2018 Macmillan Publishers Limited, part of Springer Nature. All rights reserved.

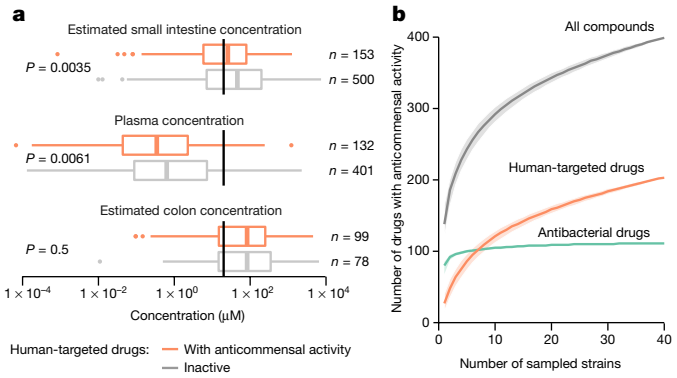

Figure 2 | Evaluating human-targeted drugs with anticommensal activity. a, Estimated small intestine and colon concentrations and measured plasma concentrations of human-targeted drugs with (orange) and without (grey) anticommensal activity in our screen (see Methods; Extended Data Fig. 3). For both active and inactive compounds, the median estimated small intestine and colon concentrations are higher than the screened concentration (20 μM, black vertical lines), whereas plasma concentrations are lower. Non-hits in our screen generally reached higher plasma and small intestine concentrations (two-sided Wilcoxon rank sum test). Box plots: centre line, median; limits, upper and lower quartiles; whiskers, 1.5× IQR; points, outliers. **b**, Rarefaction analysis indicates that anticommensal activity would be discovered for more human-targeted drugs if we screened additional strains.

systematically measured only in blood; there, human-targeted drugs have on average an order of magnitude lower concentrations than in our screen (Fig. 2a, Extended Data Fig. 3). We deduced colon concentrations on the basis of drug excretion patterns from published work, and small intestine concentrations on the basis of daily doses of individual drugs (Supplementary Table 1) and a measured example of duodenal concentrations for the well-absorbed drug posaconazole[19] (see Methods). Based on these approximations, 20 μM was below the median small intestine and colon concentration of the human-targeted drugs tested here (Fig. 2a, Extended Data Fig. 3). Notably, human-targeted drugs that showed anticommensal activity had lower plasma and estimated small intestinal concentrations than ones with no such activity (Fig. 2a; $P = 0.0061$ and $P = 0.0035$, respectively, two-sided Wilcoxon rank sum test; we have fewer colon concentration estimates owing to data availability), suggesting that more human-targeted drugs would inhibit bacterial growth if probed at higher doses, closer to physiological concentrations. A case in point is metformin, which was recently identified as the key contributor to changes in the human gut microbiome composition of patients with type II diabetes[2], but lacked anticommensal activity in our screen. Metformin reaches 10–40 μM in the plasma of treated patients with type II diabetes, but its small intestine concentration is 30–300-fold higher[20], which matches our estimates of small intestine and colon concentrations (1.5 mM). When we probed for higher, more physiological intestinal metformin concentrations, 3 of 22 tested strains were inhibited at concentrations below 1.5 mM (Extended Data Fig. 4a).

We also benchmarked our screen with an independent set of experiments, measuring IC_{25} (the drug concentration conferring 25% growth inhibition) for 25 selected drugs in a subset of up to 27 strains (see Methods). This analysis revealed excellent precision (94%), but slightly lower recall (85%) (Extended Data Fig. 5a, b). False negatives, that is, drugs with anticommensal activity missed in our screen, were due to specific chemicals that probably lost activity during screening (Extended Data Fig. 5d), and our stringent FDR cutoff for calling hits. Increasing this cutoff to 0.1 would almost double the fraction of drugs with anticommensal activity (Extended Data Fig. 5c). In addition, we found that more species were inhibited at higher concentrations (Extended Data Fig. 5d, Supplementary Table 4), and that IC_{25} values were mainly below the estimated gut concentrations and occasionally below plasma concentrations (Extended Data Fig. 6).

Furthermore, we screened only a representative subset of species, but the gut microbiome of an individual harbours hundreds of species and an even larger strain diversity[21]. Rarefaction analysis indicates that if more gut species were tested, the fraction of human-targeted drugs with anticommensal activity would increase (Fig. 2b).

In summary, we probed human-targeted drugs largely within physiologically relevant concentrations and our data are likely to under-report the impact of human-targeted drugs on gut bacteria.

Concordance with patient data

Having demonstrated that many human-targeted drugs inhibit gut bacteria *in vitro* at relevant doses, we searched for evidence that such effects manifest *in vivo* in the human gut. We reviewed all available clinical cohort data from metagenomics association studies and compared it to our screen if studies had enough statistical power and affected taxa that overlapped with those tested here. We found suitable studies for PPIs, AAPs, and seven further drugs, spanning altogether five different drug classes according to Anatomical Therapeutic Chemical (ATC) classification. All three PPI representatives in our screen exhibited broad anticommensal activity, similar to the microbiome changes that have been reported in patients taking PPIs[3,4] (Fig. 3a): taxa with reduced abundance in patients exhibited reduced growth in our screen and taxa enriched in patients were rarely inhibited by PPIs *in vitro* (Extended Data Fig. 7a). This suggests that PPIs directly influence the gut microbiome composition, in addition to changing the stomach pH and thus affecting which bacteria reach the gut[3,4]. Concordance was similarly high for many microbe–drug associations identified in a large Flemish cohort[7] for the immunosuppressive agent azathioprine, the antidepressant venlafaxine, the anti-inflammatory mesalazine, aminosalicylate, progesterone, oestrogens and amoxicillin; the only exception was another antibiotic, nitrofurantoin (Extended Data Fig. 7b, c). We also compared our data to a study that reported a reduction in *Akkermansia* levels in the gut of patients treated with AAPs[6]. Our screen included six of the ten AAPs investigated in that study. We found that *Akkermansia muciniphila* was more sensitive than other strains to these AAPs ($P = 0.09$; two-sided Wilcoxon rank sum test), while being more resistant to other human-targeted drugs ($P = 0.0005$, two-sided Wilcoxon rank sum test; Extended Data Fig. 7d). Finally, we found high concordance between a longitudinal microbiome study of patients taking metformin and our IC_{25} data for the same drug (Extended Data Fig. 4b).

Metagenomics association studies and our *in vitro* study have distinct limitations. We screened a subset of species, mostly one strain per species, out of the context of microbial communities and the host. Cohort studies can be underpowered or biased by methodological approaches and confounding factors, and may detect indirect effects. Nonetheless, we find high concordance between the effects of drugs *in vitro* and in humans, confirming clinical relevance and direct anticommensal activity for the aforementioned cases.

To assess the physiological relevance of our screen further, we investigated the registered side effects of these drugs in humans. We first identified side effects enriched in antibiotics for systemic use compared to those found in all other drugs in the SIDER database[22]. We identified 69 side effects that were enriched in antibiotics (see Methods; Supplementary Table 5). These antibiotic-related side effects occurred more often in clinical trials of human-targeted drugs with anticommensal activity than in trials of compounds that were inactive in our screen ($P = 0.002$, two-sided Wilcoxon rank sum test), whereas no significant difference was observed for placebo-treated patients (Fig. 3b). This suggests that the collateral damage of human-targeted drugs on gut bacteria can be detected by higher occurrences of antibiotic-like side effects in patients.

We then tested whether this side effect signature predicted anticommensal activity of human-targeted drugs, which we could have

© 2018 Macmillan Publishers Limited, part of Springer Nature. All rights reserved.

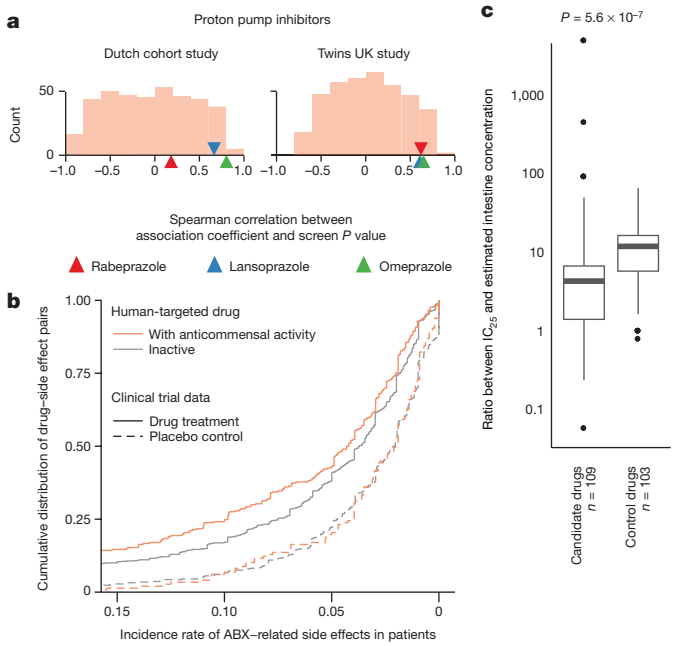

Figure 3 | Anticommensal activity of human-targeted drugs *in vitro* reflects patient data. a, Changes in microbiome composition of patients taking PPIs are consistent with drug effects in our screen. Displayed are Spearman correlation coefficients between *in vitro* growth inhibition *P* values and changes in taxonomic relative abundance after PPI consumption for corresponding taxa from two studies (Twins UK[4] and Dutch[3] cohorts; 229 of 1,827 and 211 of 1,815 individuals had taken PPIs, respectively). The histogram represents the background distribution of correlations between the *in vitro* data for all human-targeted drugs and the *in vivo* response to PPIs; correlations with PPIs are highlighted by triangles. **b**, Human-targeted drugs with anticommensal activity in our screen had a significantly higher incidence of antibiotic-related side effects (orange trace shows cumulative distribution, $n = 285$ drug–side effect pairs) in clinical trials compared to drugs without activity (grey trace, $n = 767$; $P = 0.002$, two-sided Wilcoxon rank sum test). Dashed lines indicate the incidence of the same side effects upon placebo treatment, with no significant difference between active ($n = 138$) and inactive drugs ($n = 474$). **c**, Based on similarity to antibiotic-related side effects, we selected 26 candidate and 16 control drugs for testing for anticommensal activity. Although both candidate and control drugs inhibited bacterial growth at higher concentrations, candidate drugs had anticommensal activity at significantly lower doses than control drugs after normalizing for estimated intestine concentrations ($P = 5.6 \times 10^{-7}$, two-sided Wilcoxon rank sum test). Box plots as in Fig. 2a, *n* denotes number of drug-strain pairs.

missed owing to the low drug concentration we used. We screened 26 candidate compounds that showed enrichment of antibiotic-related side effects and 16 that did not (control compounds) for effects on the growth of 18 bacterial strains (Extended Data Fig. 8), in concentrations up to 2.5 mM (Methods). Twenty-eight of these forty-two compounds inhibited the growth of at least one strain (Extended Data Fig. 8a–d), with both the fraction of active compounds and the number of affected strains being similar for both candidate and control compounds. However, when we normalized the measured IC_{25} by the estimated intestine concentration (based on the recommended single drug dose) to make amounts comparable between drugs, a significant difference was evident. Drugs that were predicted to be active had a median IC_{25} across all drug–strain pairs that corresponded to 4.3 drug doses, compared to 12 for control drugs ($P = 5.6 \times 10^{-7}$, two-sided Wilcoxon rank sum test; Fig. 3c). The IC_{25} corresponds to less than two drug doses in 34% of drugs with predicted activity, compared to just 8% for control drugs. Similarly, the IC_{25} is below the estimated colon concentration for 16/52 (31%) of candidate drug-strain pairs and for only 5/50 (10%) of control drug-strain pairs (Extended Data Fig. 8e).

In conclusion, human-targeted drugs with anticommensal activity have antibiotic-like side effects in humans, and for the few studies available, consumption of these drugs led to changes in taxa we also detected to be inhibited *in vitro*, implying that more drugs with anticommensal activity reported here will have an impact *in vivo*.

Features of drugs with anticommensal activity

Drugs from all major ATC indication areas exhibited anticommensal activity, with antineoplastics, hormones and compounds that target the nervous system inhibiting gut bacteria more than other medications (Extended Data Figs 9a, 10). Three ATC subclasses (antimetabolites, antipsychotics and calcium-channel blockers) were significantly enriched in hits (Extended Data Fig. 9a). Antimetabolites are used as chemotherapeutic and immunosuppressant agents, with their incorporation into RNA or DNA, or their interaction with synthesis enzymes being cytotoxic to human cells. Their molecular targets are often conserved in bacteria[23], explaining the observed effects and raising the possibility that antibacterial effects may also be directly involved in the development of mucositis during chemotherapy[24].

The enrichment in antipsychotics is intriguing, given that they target dopamine and serotonin receptors in the brain, which are absent in bacteria. Although phenothiazines are known to have antibacterial effects[25], nearly all subclasses of the chemically diverse antipsychotics exhibited anticommensal activity (Extended Data Fig. 9b). These drugs targeted a significantly more similar pattern of species than expected from their chemical similarity ($P = 2 \times 10^{-19}$, permutation test; Extended Data Fig. 9c). This raises the possibility that direct bacterial inhibition may not only manifest as side effect of antipsychotics[26], but also be part of their mechanism of action.

As different ATC indication areas contain chemically similar drugs, we investigated whether the chemical properties of drugs can influence their anticommensal activity (Extended Data Fig. 11a). To some degree, chemically similar human-targeted drugs had more similar effects in the screen than less similar drugs (Extended Data Fig. 11b). We tested several compound properties, including complexity, molecular weight, topological polar surface area (TPSA), volume and hydrophobicity (XLogP). Complex, heavier and larger compounds preferentially targeted Gram-positive bacteria, whereas Gram-negative bacteria were protected against such bulkier drugs by their selective outer membrane barrier (Extended Data Fig. 12). Owing to the vast number of chemical moieties present in drugs with anticommensal activity, we did not attempt an exhaustive enrichment analysis. Nevertheless, we did observe reactive nitro-groups being enriched in drugs with anticommensal activity ($P = 6.4 \times 10^{-6}$, Fisher's exact test), indicating that local chemical properties may confer antibacterial activity.

Human-targeted drugs may boost antibiotic resistance

There is a strong correlation between resistance to antibacterials and resistance to human-targeted drugs in our data that cannot be explained simply by general cell envelope composition, as there is no clear division between Gram-positive and Gram-negative bacteria (Fig. 4a). We reasoned that more specific but common mechanisms could confer resistance to both drug groups. To test this hypothesis, we selected TolC, known to efflux several antibiotics in *E. coli* and other bacteria[27], as a prominent representative of a general resistance mechanism against antibiotics. We profiled an *E. coli* Δ*tolC* mutant and its parental wild type (BW25113) against the Prestwick Chemical Library. *E. coli* lacking TolC not only became more sensitive to antibacterials (22 hits more than wild type), but also became equally more sensitive to human-targeted drugs (19 additional hits; Fig. 4a, Supplementary Table 6). This effect is not specific to *E. coli* or TolC, as a more antibiotic-resistant *B. uniformis* strain (HM-715) was also equally more resistant to human-targeted drugs (Fig. 4a).

While our data support a strong role for common general resistance mechanisms, there are also outliers to this trend, the most prominent being *C. difficile* and *P. distansonis* (Fig. 4a). For both, strong

© 2018 Macmillan Publishers Limited, part of Springer Nature. All rights reserved.

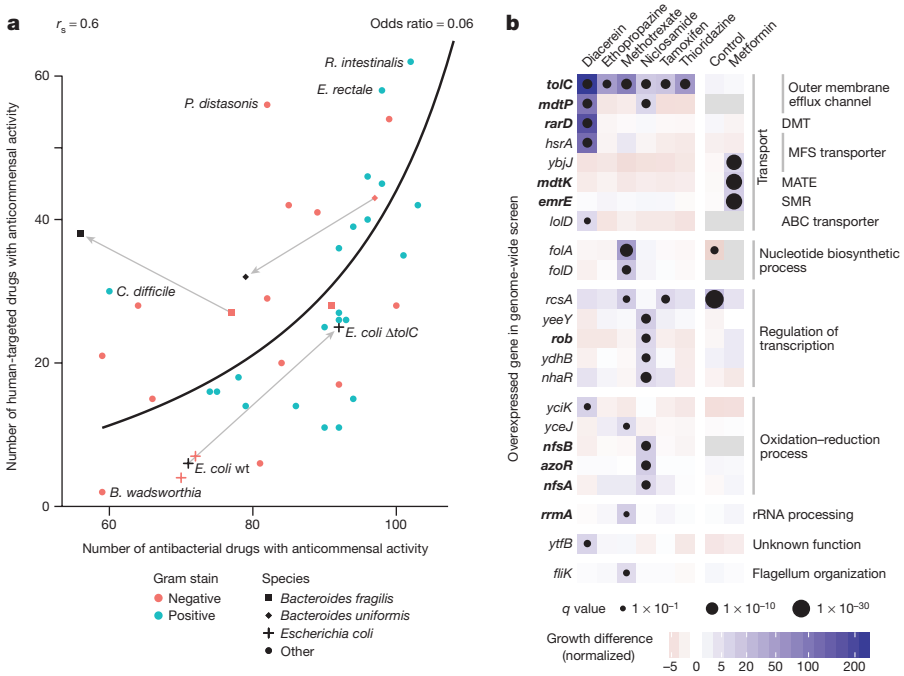

Figure 4 | Antibiotic resistance mechanisms protect against human-targeted drugs. a, Susceptibility to antibacterial agents and human-targeted drugs correlates across the 40 tested strains (Spearman correlation, $r_S = 0.6$ and a line depicting the nonlinear least-squares estimate of the odds ratio, OR = 0.06), suggesting common resistance mechanisms against both drug types. Knockout of a major antibiotic efflux pump (*tolC*) in the laboratory *E. coli* strain BW25113 (which behaves like the other two commensal *E. coli* strains in the screen) makes *E. coli* equally more sensitive to both antibacterials and human-targeted drugs. Two antibiotic-resistant isolates of *B. fragilis* (black square, HM-20) and *B. uniformis* (black diamond, HM-715) were screened in addition to the main screen, with only the latter showing a similar increase in resistance towards human-targeted drugs. **b**, Chemical genetic screen of an *E. coli* genome-wide overexpression library in seven non-antibiotics; all screens except for metformin were performed in Δ*tolC* background to sensitize *E. coli* to these drugs. Genes that when overexpressed significantly improved the growth of *E. coli* in the presence of at least one of the drugs are shown here; genes in bold have been previously associated with antibiotic resistance. Among them are genes encoding for transporters from different families: DMT (drug metabolite transporter), MFS (major facilitator superfamily), MATE (multidrug and toxin extrusion), SMR (small multidrug resistance) and ABC (ATP-binding cassette). Growth is measured by colony size (median $n = 4$)[40], colour depicts the normalized size difference from the median growth of all strains in the drug (more than sixfold difference), and dot size the significance (FDR-corrected $P < 0.1$). Control denotes the growth of the library without drug.

antibiotic resistance[28] contrasted with relatively weaker resistance to human-targeted drugs. Similarly, an antibiotic-resistant *B. fragilis* strain, HM-20, was not equally resistant against human targeted drugs (Fig. 4a). These examples make the important distinction between specific antibiotic resistance mechanisms, which are irrelevant for resistance to human-targeted drugs, and more predominant, general mechanisms, which confer resistance to both drug groups.

To elucidate mechanisms conferring resistance against human-targeted drugs more systematically, we used a chemical genetic approach[29] and screened a genome-wide overexpression library in *E. coli* against seven non-antibiotics (six human-targeted drugs and niclosamide, an antiparasitic) that showed broad anticommensal activity in our screen. As wild-type *E. coli* was one of the most resistant gut species (Fig. 4a), we used the Δ*tolC* mutant, which is sensitive to most of these drugs, allowing us to probe further resistance mechanisms. For all tested drugs except metformin, overexpression of *tolC* rescued *E. coli* growth, as expected. Furthermore, we identified a number of diverse transporter families that contributed to resistance against these drugs (Fig. 4b). Many of them have previously been linked to antibiotic resistance[30–33]. Resistance was also acquired by overexpression of transcription factors (for example, *rob*, which controls efflux pump expression[34]), the ribosome maturation factor *rrmA*, which plays a role in resistance to the antibiotic viomycin[35], and detoxification mechanisms (nitroreductases modify nitro-containing antibiotics[36]). For methotrexate, we validated the known primary target in bacteria (*E. coli* dihydrofolate reductase)[37], illustrating the potential of this approach to identify bacterial mechanism of action of human-targeted drugs[29].

All of these results point to an overlap between resistance mechanisms against antibiotics and against human-targeted drugs, implying a hitherto unnoticed risk of acquiring antibiotic resistance by consuming non-antibiotic drugs.

Discussion

We report a systematic drug screen against a reference panel of human gut bacteria. Twenty-seven per cent of non-antibiotics (24% of human-targeted drugs) inhibited the growth of at least one species. As we demonstrated, this is likely to be an underestimate owing to stringent thresholds for calling hits and the limited selection of bacterial strains screened. Many of the direct *in vitro* effects described here may translate into microbiome shifts *in vivo*, because (i) we used concentrations within the range of what is estimated to be found in the human gut for many drugs; (ii) our observations agree with the few clinical microbiome studies for which medication has been recorded; and (iii) the side effects of anticommensal drugs in humans resemble those of antibiotics. Thus, our results underscore the necessity of accounting for potential medication-related confounding effects in future microbiome disease association studies. Moreover, one could speculate that pharmaceuticals, used regularly in our times, may be contributing to a decrease in microbiome diversity in modern Western societies[38].

Although the antibacterial potential of human-targeted drugs has been profiled repeatedly in the quest for new antimicrobials, previous efforts have focused on pathogenic and often multi-drug-resistant (MDR) bacterial species[9,13,14]. We demonstrate that some of these species or their commensal relatives are the most drug-resistant in our screen (for example, γ-proteobacteria: *Bilophila wadsworthia* and *E. coli* were affected by 2 and 4–7 human targeted drugs, respectively), that many human-targeted drugs have species-specific effects, and that resistance mechanisms to antibiotics and human-targeted drugs

© 2018 Macmillan Publishers Limited, part of Springer Nature. All rights reserved.

partially overlap (thus, MDR species may be more resistant to human drugs too). Together, these findings explain why previous efforts have failed to register how many human-targeted drugs can inhibit bacteria.

Many pharmaceuticals influence the human gut microbiota. As gut bacteria, in turn, can also modulate drug efficacy and toxicity[39], the emerging drug–microbe network could guide therapy and drug development. The resource described here opens up new avenues for translational applications in mitigating drug side effects, improving drug efficacy, repurposing of human-targeted drugs as antibacterials or microbiome modulators, and controlling antibiotic resistance (see Supplementary Discussion). However, before any translational application can be pursued, our *in vitro* findings need to be tested rigorously *in vivo* (in animal models, pharmacokinetic studies and clinical trials) and understood better mechanistically.

Online Content Methods, along with any additional Extended Data display items and Source Data, are available in the online version of the paper; references unique to these sections appear only in the online paper.

Received 26 March 2017; accepted 8 February 2018.
Published online 19 March 2018.

1. Kåhrström, C. T., Pariente, N. & Weiss, U. Intestinal microbiota in health and disease. *Nature* **535,** 47 (2016).
2. Forslund, K. *et al.* Disentangling type 2 diabetes and metformin treatment signatures in the human gut microbiota. *Nature* **528,** 262–266 (2015).
3. Imhann, F. *et al.* Proton pump inhibitors affect the gut microbiome. *Gut* **65,** 740–748 (2016).
4. Jackson, M. A. *et al.* Proton pump inhibitors alter the composition of the gut microbiota. *Gut* **65,** 749–756 (2016).
5. Rogers, M. A. & Aronoff, D. M. The influence of non-steroidal anti-inflammatory drugs on the gut microbiome. *Clin. Microbiol. Infect.* **22,** 171–179 (2016).
6. Flowers, S. A., Evans, S. J., Ward, K. M., McInnis, M. G. & Ellingrod, V. L. Interaction between atypical antipsychotics and the gut microbiome in a bipolar disease cohort. *Pharmacotherapy* **37,** 261–267 (2017).
7. Falony, G. *et al.* Population-level analysis of gut microbiome variation. *Science* **352,** 560–564 (2016).
8. Tramontano, M. *et al.* Nutritional preferences of the human gut bacteria reveal their metabolic idiosyncasies. *Nat. Microbiol.* https://doi.org/10.1038/s41564-018-0123-9 (2018).
9. Ejim, L. *et al.* Combinations of antibiotics and nonantibiotic drugs enhance antimicrobial efficacy. *Nat. Chem. Biol.* **7,** 348–350 (2011).
10. Taber, H. W., Mueller, J. P., Miller, P. F. & Arrow, A. S. Bacterial uptake of aminoglycoside antibiotics. *Microbiol. Rev.* **51,** 439–457 (1987).
11. Blaser, M. J. Antibiotic use and its consequences for the normal microbiome. *Science* **352,** 544–545 (2016).
12. Rani, N., Sharma, A. & Singh, R. Imidazoles as promising scaffolds for antibacterial activity: a review. *Mini Rev. Med. Chem.* **13,** 1812–1835 (2013).
13. Harbut, M. B. *et al.* Auranofin exerts broad-spectrum bactericidal activities by targeting thiol-redox homeostasis. *Proc. Natl Acad. Sci. USA* **112,** 4453–4458 (2015).
14. Farha, M. A. *et al.* Antagonism screen for inhibitors of bacterial cell wall biogenesis uncovers an inhibitor of undecaprenyl diphosphate synthase. *Proc. Natl Acad. Sci. USA* **112,** 11048–11053 (2015).
15. Pasolli, E., Truong, D. T., Malik, F., Waldron, L. & Segata, N. Machine learning meta-analysis of large metagenomic datasets: tools and biological insights. *PLOS Comput. Biol.* **12,** e1004977 (2016).
16. Koh, A., De Vadder, F., Kovatcheva-Datchary, P. & Bäckhed, F. From dietary fiber to host physiology: short-chain fatty acids as key bacterial metabolites. *Cell* **165,** 1332–1345 (2016).
17. Arumugam, M. *et al.* Enterotypes of the human gut microbiome. *Nature* **473,** 174–180 (2011).
18. Donaldson, G. P., Lee, S. M. & Mazmanian, S. K. Gut biogeography of the bacterial microbiota. *Nat. Rev. Microbiol.* **14,** 20–32 (2016).
19. Hens, B., Brouwers, J., Corsetti, M. & Augustijns, P. Supersaturation and precipitation of posaconazole upon entry in the upper small intestine in humans. *J. Pharm. Sci.* **105,** 2677–2684 (2016).
20. Bailey, C. J., Wilcock, C. & Scarpello, J. H. Metformin and the intestine. *Diabetologia* **51,** 1552–1553 (2008).
21. Schloissnig, S. *et al.* Genomic variation landscape of the human gut microbiome. *Nature* **493,** 45–50 (2013).
22. Kuhn, M., Letunic, I., Jensen, L. J. & Bork, P. The SIDER database of drugs and side effects. *Nucleic Acids Res.* **44,** D1075–D1079 (2016).
23. Bodet, C. A., III, Jorgensen, J. H. & Drutz, D. J. Antibacterial activities of antineoplastic agents. *Antimicrob. Agents Chemother.* **28,** 437–439 (1985).
24. Stringer, A. M., Gibson, R. J., Bowen, J. M. & Keefe, D. M. Chemotherapy-induced modifications to gastrointestinal microflora: evidence and implications of change. *Curr. Drug Metab.* **10,** 79–83 (2009).
25. Sharma, S. & Singh, A. Phenothiazines as anti-tubercular agents: mechanistic insights and clinical implications. *Expert Opin. Investig. Drugs* **20,** 1665–1676 (2011).
26. Morgan, A. P. *et al.* The antipsychotic olanzapine interacts with the gut microbiome to cause weight gain in mouse. *PLoS One* **9,** e115225 (2014).
27. Li, X. Z., Plésiat, P. & Nikaido, H. The challenge of efflux-mediated antibiotic resistance in Gram-negative bacteria. *Clin. Microbiol. Rev.* **28,** 337–418 (2015).
28. Nagy, E., Urbán, E., Nord, C. E. & ESCMID Study Group on Antimicrobial Resistance in Anaerobic Bacteria Antimicrobial susceptibility of *Bacteroides fragilis* group isolates in Europe: 20 years of experience. *Clin. Microbiol. Infect.* **17,** 371–379 (2011).
29. Cacace, E., Kritikos, G. & Typas, A. Chemical genetics in drug discovery. *Curr. Op. Syst. Biol.* **4,** 35–42 (2017).
30. Morita, Y. *et al.* NorM, a putative multidrug efflux protein, of *Vibrio parahaemolyticus* and its homolog in *Escherichia coli*. *Antimicrob. Agents Chemother.* **42,** 1778–1782 (1998).
31. Sulavik, M. C. *et al.* Antibiotic susceptibility profiles of *Escherichia coli* strains lacking multidrug efflux pump genes. *Antimicrob. Agents Chemother.* **45,** 1126–1136 (2001).
32. Nichols, R. J. *et al.* Phenotypic landscape of a bacterial cell. *Cell* **144,** 143–156 (2011).
33. Nasie, I., Steiner-Mordoch, S. & Schuldiner, S. New substrates on the block: clinically relevant resistances for EmrE and homologues. *J. Bacteriol.* **194,** 6766–6770 (2012).
34. Ariza, R. R., Li, Z., Ringstad, N. & Demple, B. Activation of multiple antibiotic resistance and binding of stress-inducible promoters by *Escherichia coli* Rob protein. *J. Bacteriol.* **177,** 1655–1661 (1995).
35. Gustafsson, C. & Persson, B. C. Identification of the rrmA gene encoding the 23S rRNA m1G745 methyltransferase in *Escherichia coli* and characterization of an m1G745-deficient mutant. *J. Bacteriol.* **180,** 359–365 (1998).
36. Roldán, M. D., Pérez-Reinado, E., Castillo, F. & Moreno-Vivián, C. Reduction of polynitroaromatic compounds: the bacterial nitroreductases. *FEMS Microbiol. Rev.* **32,** 474–500 (2008).
37. Matthews, D. A. *et al.* Dihydrofolate reductase: x-ray structure of the binary complex with methotrexate. *Science* **197,** 452–455 (1977).
38. Clemente, J. C. *et al.* The microbiome of uncontacted Amerindians. *Sci. Adv.* **1,** e1500183 (2015).
39. Spanogiannopoulos, P., Bess, E. N., Carmody, R. N. & Turnbaugh, P. J. The microbial pharmacists within us: a metagenomic view of xenobiotic metabolism. *Nat. Rev. Microbiol.* **14,** 273–287 (2016).
40. Kritikos, G. *et al.* A tool named Iris for versatile high-throughput phenotyping in microorganisms. *Nat. Microbiol.* **2,** 17014 (2017).

Supplementary Information is available in the online version of the paper.

Acknowledgements We thank P. Beltrao (EBI), K. C. Huang (Stanford) and F. Cabreiro (UCL) for feedback on the manuscript; F. Rippmann (Merck KGaA) for pointing to the delayed onset of antipsychotics; S. Wicha (University of Hamburg) for discussions on drug concentrations; J. Overington (Medicines Discovery Catapult) for help with drug plasma concentrations, and members of all four laboratories for fruitful discussions (in particular T. Hodges for suggestions on the manuscript and M. Driessen for experimental support). We thank the EMBL mechanical workshop for the custom-made incubator. We acknowledge funding from EMBL and the Microbios grant (ERC-AdG-669830). L.M. and M.P. were supported by the EMBL Interdisciplinary Postdoc (EIPOD) programme under Marie Sklodowska Curie Actions COFUND (grant 291772). A.Te. and A.R.B. were supported by a Sofja Kovaleskaja Award of the Alexander von Humboldt Foundation to A.Ty.

Author Contributions The study was conceived by K.R.P., P.B. and A.Ty., designed by L.M., M.P., G.Z., A.R.B. and A.Ty., and supervised by K.R.P., P.B. and A.Ty. *In vitro* screening was established by M.P. and performed by L.M., M.P., A.Te. and K.C.F. Follow-up and validation experiments were conducted by L.M., M.P. and E.E.A. H.D. and H.M. constructed and provided the Transbac library. Data preprocessing was performed by M.K. and G.Z.; statistical analyses by M.K.; data curation by L.M., M.K. and E.E.A.; data interpretation by L.M., M.P., M.K., G.Z., K.R.P., P.B. and A.Ty. L.M., M.K., G.Z., K.R.P., P.B. and A.Ty. wrote the manuscript with input from M.P. and A.R.B.; L.M., M.K. and G.Z. designed figures with input from K.R.P., P.B. and A.Ty. All authors approved the final version for publication.

Author Information Reprints and permissions information is available at www.nature.com/reprints. The authors declare competing financial interests: details are available in the online version of the paper. Readers are welcome to comment on the online version of the paper. Publisher's note: Springer Nature remains neutral with regard to jurisdictional claims in published maps and institutional affiliations. Correspondence and requests for materials should be addressed to A.Ty. (typas@embl.de), G.Z. (zeller@embl.de), K.R.P. (patil@embl.de) and P.B. (bork@embl.de).

Reviewer Information *Nature* thanks K. Lewis, H. B. Nielsen, G. Wright and R. Xavier for their contribution to the peer review of this work.

© 2018 Macmillan Publishers Limited, part of Springer Nature. All rights reserved.

METHODS

Bacterial strains and growth conditions. Bacterial isolates used in this study were purchased from DSMZ, BEI Resources, ATCC and Dupont Health & Nutrition, or were gifts from the Denamur Laboratory (INSERM). All strains were recovered in their recommended rich medium (resource and literature). The screen and validation experiments were performed in mGAM (HyServe GmbH & Co.KG, Germany, produced by Nissui Pharmaceuticals)[41], as almost all species could grow robustly in this medium in a manner that is reflective of their gut abundance[8]. Because we selected for robust growth, potential positive effects of drugs on growth could not be detected. Only one strain was grown in Todd-Hewitt Broth (Sigma-Aldrich), one in a 1:1 mixture of mGAM and gut microbiota medium[42] and, for one strain, mGAM was supplemented with 60 mM sodium formate and 10 mM taurine (see also Supplementary Table 2). All media were pre-reduced at least 1 day before use under anoxic conditions in an anaerobic chamber (Coy Laboratory Products Inc.) (2% H_2, 12% CO_2, rest N_2) and all experiments were performed under anaerobic conditions at 37 °C unless specified otherwise. No statistical methods were used to predetermine sample size.

Species selection. To select a representative core of species in the human gut microbiome, we analysed 364 fecal metagenomes from asymptomatic individuals from three continents[43–46]. Species were defined and their abundance quantified as previously described[47,48]. A core set of 60 microbiome species was defined (Extended Data Fig. 1b–d), and from this core, 31 species were selected for this screen. Seven additional species were selected for reasons explained in the main text.

Screen of the Prestwick Chemical Library. *Preparation of screening plates.* The Prestwick Chemical Library was purchased from Prestwick Chemical Inc. with compounds coming dissolved in dimethyl sulfoxide (DMSO) at a concentration of 10 mM. Compounds were re-arrayed to redistribute the DMSO control wells in each plate and to minimize the total number of 96- and 384-well plates (4 × 384-well plates or 14 × 96-well plates). At the same time, drugs were diluted to a concentration of 2 mM to facilitate further aliquoting, and these plates were stored at −30 °C. For each experimental batch (10 replicates in 96-well plates; 20 replicates in 384-well plates), we prepared drug plates in the respective growth medium (2× for 96-well plates, 1× for 384-well plates), and stored them at −30 °C until use (maximum 2 months). Before inoculation, plates were thawed and pre-reduced in the anaerobic chamber overnight. The Biomek FXP (Beckman Coulter) liquid handling system was used for all rearranging and aliquoting of the library compounds.

Inoculation. Strains were grown twice overnight to make sure we had a robustly and uniformly growing culture before inoculating the screening plates. For 96-well plates, the second overnight culture was diluted to fresh medium in order to reach 2× the desired starting optical density (OD) at 578 nm. Next, 50 μl of this diluted inoculum was added to wells containing 50 μl of 2× concentrated drug in the respective culture medium using a multichannel pipetter. The final drug concentration was 20 μM and each well contained 1% DMSO. We inoculated 384-well plates with a 384 floating pin replicator VP384FP6S (V&P Scientific, Inc.), transferring 1 μl of appropriately diluted overnight culture to wells containing 50 μl of growth medium, 1% DMSO and 20 μM drug. For bacterial species that reached lower OD in overnight cultures we transferred twice 1 μl of appropriately adjusted OD culture. For both 96- and 384-well plates, the starting OD was 0.01 or 0.05, depending on the growth preference of the species (Supplementary Table 2).

Screening conditions. After inoculation, plates were sealed with breathable membranes (Breathe-Easy) to prevent evaporation and cross-contamination between wells, and incubated at 37 °C without shaking. Growth curves were acquired by tracking OD at 578 nm with a microplate spectrophotometer (EON, Biotek). Measurements were taken every 1–3 h after 30–60 s of linear shaking, initially manually but later automatically using a microplate stacker (Biostack 4, Biotek), fitted inside a custom-made incubator (EMBL Mechanical Workshop). We collected measurements for 16–24 h. Each strain was screened in at least three biological replicates.

Normalization of growth curves and quantification of growth. Growth curves were analysed by plate. All growth curves within a plate were truncated at the time of transition from exponential to stationary phase. The end of the exponential phase was determined automatically by finding the peak OD (using the median across all compounds and control wells, and accounting for a small increase during the stationary phase) and verified by inspection. Using this time point allowed us to capture the effects of drugs on lag phase, growth rate and stationary phase plateau (Extended Data Fig. 2a). Time points with sudden spikes in OD (for example, caused by condensation) were removed, and growth curves were discarded completely if they had too many missing time points (Extended Data Fig. 2a). Similarly, growth curves were discarded if the OD fell far outside the normal range (for example, caused by coloured compounds). Three compounds had to be completely excluded from the analysis, as they caused aberrant growth curves: Chicago sky blue 6B, mitoxantrone and verteporfin.

Growth curves were processed by plate to set the median OD at the start and end time points to 0 and 1, respectively. Then we defined reference compounds across all replicates as those that did not reduce growth significantly for most drugs, had measurements for >95% of all replicates, and for which the final OD was >0.5 for more than 142 out of 152 replicates. We used these reference compounds as representatives of uninhibited growth. As wells containing reference compounds outnumbered control wells within a plate, we used control wells only later to verify the *P* value calculation (Extended Data Fig. 2d). After identifying reference compounds, we rescaled growth curves such that the median growth of reference compounds at the end point was 1.

While growth curves in control wells and most wells with reference compounds followed the expected logistic growth pattern, a variety of deviations were observed for drugs that influenced growth. To quantify growth without relying on assumptions about the shape of the growth curve, we calculated the area under the curve (AUC) using the trapezoidal rule. Although we set the median starting OD to 0, the ODs of individual wells deviated from this. We used two methods to correct for this and determine the baseline for each growth curve (Extended Data Fig. 2a). First, a constant shift was assumed, subtracting the same shift from all time points of the growth curve such that the minimum is zero. Second, an initial perturbation was assumed that affects initial time points more than later time points (for example, condensation). To correct this, we first subtracted a constant shift as above, and then rescaled the curve such that a time point with an uncorrected OD of 1 also had an OD of 1 after correction. AUCs were calculated for both scenarios, rescaled such that the AUC of reference compounds was 1, and then for each compound the baseline correction that yielded an AUC closest to 1 (that is, normal growth) was selected.

AUCs are highly correlated to final ODs, with a Pearson correlation of 0.95 across all compounds and replicates. Nonetheless, we preferred to use AUCs to decrease the influence of the final time point, which will contain more noise than a metric based on all time points.

Identification of drugs with anticommensal activity. We detected hits from normalized AUC measurements using a statistical method that controls for multiple hypothesis testing and varying data quality. We fitted heavy-tailed distributions (scaled Student's *t*-distribution[49]) to the wells containing reference compounds for each replicate and, separately, to each individual plate. These distributions captured the range of AUCs expected for compounds that did not reduce growth, and represented the null hypothesis that a given drug did not cause a growth defect in the given replicate or plate. We calculated one-sided *P* values from the cumulative distribution function of the fitted distribution. Within a replicate, each compound was associated with two *P* values: one from the plate on which it was measured, and one for the whole replicate. Of those two, the highest *P* value was chosen (conservative estimate) to control for plates with little or high noise, and varying levels of noise within the same replicate.

The resulting *P* values were well-calibrated (that is, the distribution of *P* values was close to uniform with the exception of a peak at low *P* values, Extended Data Fig. 2d) and captured the distribution of controls, which were not used for fitting the distribution and kept for validation. We then combined *P* values for a given drug and strain across replicates using Fisher's method. Lastly, we calculated the FDR using the Benjamini–Hochberg method[50] over the complete matrix of *P* values (1,197 compounds by 40 strains). After inspecting representative AUCs for compound–strain pairs at different FDR levels, we chose a conservative FDR cut-off of 0.01.

Drug indications, dose, and administration. We annotated drugs by their primary target organism on the basis of their WHO ATC classification, or, if there were uncertainties, based on manual annotation. Compounds were classified as: antibacterial drugs (antibiotics, antiseptics), anti-infective drugs (acting against protozoa, fungi, parasites or viruses), human-targeted drugs (that is, drugs whose mechanism of action affects human cells), veterinary drugs (used exclusively in animals), and finally non-drugs (which can be drug metabolites, drugs used only in research, or endogenous substances). If a human-use drug belonged to several classes, the drug class was picked according to this order of priority (from high to low): antibacterial, anti-infective, and human-targeted drug. This ensured that drugs used also as antibacterials were not classified in the other two categories.

Drugs from the Prestwick Chemical Library were matched against STITCH 4 identifiers[51] using CART[52]. Identifiers that could not be mapped were annotated manually. Information about drug indications, dose and administration was extracted from the ATC classification system and Defined Daily Dose (DDD) database. Dose and administration data were also extracted from the Drugs@FDA resource. Doses that were given in grams were converted to mol using the molecular weight stated in the Prestwick library information files. When the dose guidelines mentioned salt forms, we manually substituted the molecular weight. Dose data from Drugs@FDA stated the amount of drug for a single dose (for example, a single tablet). Analysing the intersection between Drugs@FDA and DDD, we found that the median ratio between the single and daily doses was two. To combine the two data sets we therefore estimated the single dose as half of the daily dose (Supplementary Table 1).

© 2018 Macmillan Publishers Limited, part of Springer Nature. All rights reserved.

In general, it is difficult to estimate effective drug concentrations in the intestine, as those depend on the dose, the speed of dissolution, uptake and metabolization by human cells and by bacteria, binding to proteins, and excretion mechanisms into the gut. To estimate gut concentrations of drugs based on their dose with a simple model, we relied on an *in situ* study for posaconazole[19]. When 40 mg (57 μmol) of the drug is delivered to the stomach in either an acidic or a neutral solution, the maximum concentration in the duodenum reaches 26.3 ± 10.3 or 13.6 ± 5.8 μM, respectively. This is equivalent to dissolving the drug in 300 ml (240 ml of water to swallow the pill as recommended for bioavailability/bioequivalence studies plus ~43 ml resting water in the small intestine[53]) and an absorption rate of 90%. We collected doses for as many human-targeted drugs as we could find and used the above assumption to estimate small intestine concentrations. To estimate colon concentrations, we relied on reported fecal excretion data (Supplementary Table 1, gathered from DrugBank 5.0[54] and across the literature) assuming a single daily dose, 24 h transit time[55] and a volume of distribution in the colon of 0.6 l[56] (Extended Data Fig. 3).

IC_{25} determination and screen validation. To validate our screen, we selected 25 drugs including human-targeted drugs (19), antiprotozoals (3), one antiparasitic, one antiviral and one 'non-drug' compound. The human-targeted drugs spanned five therapeutic classes (ATC codes A, G, L, M and N). Our selection comprised mostly drugs with extended antibacterial activity in our screen (19 drugs hit >10 strains). This bias ensured that we could also evaluate false positives. We chose 15 strains to test IC_{25}s (that is the minimal concentration of drug that causes 25% growth inhibition), spanning different phyla (5) and including both sensitive (*E. rectale*, *R. intestinalis*) and resistant species (*E. coli* ED1a).

Compounds for validation were purchased from independent sources (Supplementary Table 1) and dissolved at 100× starting concentration in DMSO. Twofold serial dilutions were prepared in 96-well U-bottom plates (as for the screen). Each row contained a different drug at eleven twofold dilutions and a control DMSO well in the middle of the row (in total eight drugs per plate). These master plates were diluted to 2× assay concentration and 2% DMSO in mGAM (50 μl) and stored at −30 °C (<1 month). For the assay, plates were pre-reduced overnight in the anaerobic chamber, and mixed with an equal volume (50 μl) of appropriately diluted overnight culture (prepared as described for screening section) to reach a starting OD_{578} of 0.01 and a DMSO concentration of 1% across all wells. OD_{578} was measured hourly for 24 h after 1 min of shaking. Experiments were performed in two biological replicates.

Growth curves were converted to AUCs as described above, using in-plate control wells (no drug) to define normal growth. For each concentration, we calculated the mean across the two replicates. We further enforced monotonicity to conservatively remove noise effects: if the AUC decreased for lower concentrations, it was set to the highest AUC measured at higher concentrations. The IC_{25} was defined as the lowest concentration for which a mean AUC of below 0.75 was measured. In 68% of cases, IC_{25}s were equal between replicates and in a further 22%, there was a twofold change between replicates, which is within the twofold error margin reported for inhibitory concentrations[57]. Additionally, MIC as listed in Supplementary Table 4 was defined as the lowest concentration for which the AUC dropped below 0.1. In the large-scale screen, we detected significant growth reductions, which do not necessarily correspond to complete growth inhibition (Extended Data Fig. 2b). To ensure comparability between the results of the validation procedure and the screen, we used the IC_{25} metric for benchmarking. As inhibitory concentration calculations are known to have a twofold error margin[57], we considered an IC_{25} of 10–40 μM as being in agreement with the screening result (Extended Data Fig. 5a, b). A higher number of false negatives implies that more human-targeted drugs are likely to have anticommensal activity.

Analysis of side effects. Side effects of drugs were extracted from the SIDER 4.1 database[22] using the mapping between Prestwick compounds and STITCH 4 identifiers described above. In SIDER, side effects are encoded using the MedDRA terminology, which contains lower-level terms and preferred terms. Of these, we used the preferred terms, which are more general. We excluded rare side effects that occurred for fewer than five drugs from the analysis. Drugs with fewer than seven associated side effects were discarded[58]. In a first pass, we identified side effects associated with antibiotics in SIDER, by calculating for each side effect its enrichment for systemic antibiotics (ATC code J01) versus all other drugs using Fisher's exact test (*P* value cut-off: 0.05, correcting for multiple hypothesis testing using the Benjamini–Hochberg method). Antibiotics are typically administered in relatively high doses, and some of the enriched side effects might therefore be caused by a dose-dependent effect (for example, kidney toxicity). We therefore used an ANOVA (type II) to test whether the presence of side effects for a drug was more strongly associated with it being an antibiotic or with its (log-transformed) dose. Side effects that were more strongly associated with the dose were excluded from the list of antibiotic-related side effects.

Data on the incidence rates of side effects in patients was also extracted from SIDER 4.1. As different clinical trials can report different incidence rates, we computed the median incidence rate per drug–side effect pair. As SIDER also contains data on the incidence of side effects upon placebo treatment, we were able to ensure the absence of systematic biases.

Experimental validation of side effect-based predictions. Selected candidate and control compounds belonged to multiple therapeutic classes (ATC codes A, B, C, G, H, L, M, N, S for candidate compounds and A, C, D, G, H, M N, R, S, V for control compounds). Compounds of interest were purchased from independent sources (Supplementary Table 1) and if possible, dissolved at 5 mM concentration in mGAM. Lower concentrations were used when the solubility limit was reached. Solutions were sterile filtered, and three fourfold serial dilutions were arranged in 96-well plates, aiming at covering a broad range of drug concentrations. Inoculation and growth curve acquisition was performed as described for the IC_{25} determination experiments.

Chemical genetics in *E. coli*. *Conjugation of the TransBac overexpression plasmid library into E. coli ΔtolC.* The TransBac library, a new *E. coli* overexpression library based on a single-copy vector[59] (H.D. and H.M., unpublished resource) was conjugated in the BW25113 *ΔtolC::Kan* strain. The receiver strain (BW25113 *ΔtolC::kan*) was grown to stationary phase in LB medium, diluted to an OD_{578} of 1, and 200 μl was spread on an LB plate supplemented with 0.3 mM diaminopimelic acid (DAP). Plates were dried for 1 h at 37 °C and then a 1536 colony array of the library carried within a donor strain (BW38029 Hfr (CIP8 *oriT::cat*) *dap*$^-$ [60]) was pinned on top of the lawn. Conjugation was carried out at 37 °C for ~6 h, and the first selection was done by pinning on LB plates supplemented with tetracycline only (10 μg/ml) and growing overnight. Two more rounds of selection followed on LB plates containing both tetracycline (10 μg/ml) and kanamycin (30 μg/ml) to ensure killing of parental strains and select only for *tolC* mutants carrying the different plasmids.

Chemical genetic screen. The screen was carried out under aerobic conditions on solid LB Lennox medium (Difco), supplemented with 30 μg/ml kanamycin, 10 μg/ml tetracycline, the appropriate drug, and 0 or 100 μM IPTG. Drugs were used at the following sub-inhibitory concentrations for the *tolC* mutant: diacerein 20 μM, ethopropazine hydrochloride 160 μM, tamoxifen citrate 20 μM, niclosamide 1.25 μM, thioridazine hydrochloride 40 μM, methotrexate 320 μM, or for the wild type: metformin 100 mM. The 1536 colony array of BW25113 *ΔtolC::kan* mutant carrying the TransBac collection was pinned on the drug-containing plates, and plates were incubated for 16–38 h at 37 °C. In the case of metformin we used the version of the TransBac library in which each plasmid complements its corresponding barcoded single-gene deletion mutant[59], since we did not need to use the *ΔtolC* background to sensitize the cell. Growth of this library was determined at 0 and 100 mM metformin (both in the presence of 0, 50 and 100 μM IPTG). All plates were imaged using an 18-megapixel Canon Rebel T3i and images were processed using the Iris software[40].

Data analysis. We used colony size to measure the fitness of the mutants on the plate. For standardization of colony sizes, we subtracted the median colony size and then divided by a robust estimate of the s.d. (removing outliers below the 1st and above the 99th percentile). We found edge effects affecting up to five rows and columns around the perimeter of the plate. We therefore first standardized colony sizes across the whole plate using only colony sizes from the inner part of the plate as reference. To remove the edge effects, we subtracted from each column its median colony size, and then from each row its median colony size. Finally, we standardized the adjusted colony sizes using the whole plate as reference. The distribution of adjusted colony sizes was right-skewed (that is, more outlier colonies with larger sizes), suggesting a log-normal distribution. At the same time, the presence of outliers suggested that a logarithmic equivalent of the Student's *t*-distribution with variable degree of freedom[49] would be more suitable. We fitted such a distribution for each plate and calculated *P* values for both tails of the distribution. This approach assumes that the overexpression of most genes does not affect growth in response to drug treatment. *P* values were combined using Fisher's method across replicates and IPTG concentrations (since we noticed that different IPTG concentrations resulted in largely the same results—that is, plasmids are leaky). We corrected for multiple hypothesis testing for each drug individually using the Benjamini–Hochberg method[50].

Analysis of common resistance mechanisms. To determine a relationship between the number of human-targeted drugs (*h*) and the number of antibacterial drugs (*a*) that affect each strain, we determined the odds ratio (OR):

$$\mathrm{OR} = \frac{\frac{h}{H-h}}{\frac{a}{A-a}}$$

© 2018 Macmillan Publishers Limited, part of Springer Nature. All rights reserved.

where $H = 203$ and $A = 122$ are the numbers of human-targeted and antibacterial drugs that show activity against any strain, respectively. We computed the nonlinear least-squares estimate for OR using the following equation:

$$\frac{h}{H-h} = \mathrm{OR} \times \frac{a}{A-a}$$

Data availability. Data are available from FigShare: http://dx.doi.org/10.6084/m9.figshare.4813882. All data generated during this study are included in this published article and its Supplementary Information files.

Code availability. Scripts for analysing data and generating figures are available at https://git.embl.de/mkuhn/drug_impact_gut_bacteria. A snapshot of the repository has been deposited together with the data.

41. Rettedal, E. A., Gumpert, H. & Sommer, M. O. Cultivation-based multiplex phenotyping of human gut microbiota allows targeted recovery of previously uncultured bacteria. *Nat. Commun.* **5,** 4714 (2014).
42. Goodman, A. L. *et al.* Extensive personal human gut microbiota culture collections characterized and manipulated in gnotobiotic mice. *Proc. Natl Acad. Sci. USA* **108,** 6252–6257 (2011).
43. Qin, J. *et al.* A human gut microbial gene catalogue established by metagenomic sequencing. *Nature* **464,** 59–65 (2010).
44. Qin, J. *et al.* A metagenome-wide association study of gut microbiota in type 2 diabetes. *Nature* **490,** 55–60 (2012).
45. Human Microbiome Project Consortium. Structure, function and diversity of the healthy human microbiome. *Nature* **486,** 207–214 (2012).
46. Nielsen, H. B. *et al.* Identification and assembly of genomes and genetic elements in complex metagenomic samples without using reference genomes. *Nat. Biotechnol.* **32,** 822–828 (2014).
47. Mende, D. R., Sunagawa, S., Zeller, G. & Bork, P. Accurate and universal delineation of prokaryotic species. *Nat. Methods* **10,** 881–884 (2013).
48. Kultima, J. R. *et al.* MOCAT2: a metagenomic assembly, annotation and profiling framework. *Bioinformatics* **32,** 2520–2523 (2016).
49. Kruschke, J. K. Bayesian estimation supersedes the t test. *J. Exp. Psychol. Gen.* **142,** 573–603 (2013).
50. Benjamini, Y. & Hochberg, Y. Controlling the false discovery rate: a practical and powerful approach to multiple testing. *J. R. Stat. Soc. B* **57,** 289–300 (1995).
51. Kuhn, M. *et al.* STITCH 4: integration of protein-chemical interactions with user data. *Nucleic Acids Res.* **42,** D401–D407 (2014).
52. Deghou, S. *et al.* CART-a chemical annotation retrieval toolkit. *Bioinformatics* **32,** 2869–2871 (2016).
53. Mudie, D. M. *et al.* Quantification of gastrointestinal liquid volumes and distribution following a 240 mL dose of water in the fasted state. *Mol. Pharm.* **11,** 3039–3047 (2014).
54. Law, V. *et al.* DrugBank 4.0: shedding new light on drug metabolism. *Nucleic Acids Res.* **42,** D1091–D1097 (2014).
55. Kim, E. R. & Rhee, P. L. How to interpret a functional or motility test—colon transit study. *J. Neurogastroenterol. Motil.* **18,** 94–99 (2012).
56. Pritchard, S. E. *et al.* Fasting and postprandial volumes of the undisturbed colon: normal values and changes in diarrhea-predominant irritable bowel syndrome measured using serial MRI. *Neurogastroenterol. Motil.* **26,** 124–130 (2014).
57. Turnidge, J. & Paterson, D. L. Setting and revising antibacterial susceptibility breakpoints. *Clin. Microbiol. Rev.* **20,** 391–408 (2007).
58. Campillos, M., Kuhn, M., Gavin, A. C., Jensen, L. J. & Bork, P. Drug target identification using side-effect similarity. *Science* **321,** 263–266 (2008).
59. Otsuka, Y. *et al.* GenoBase: comprehensive resource database of *Escherichia coli* K-12. *Nucleic Acids Res.* **43,** D606–D617 (2015).
60. Mori, H. *et al.* Identification of essential genes and synthetic lethal gene combinations in *Escherichia coli* K-12. *Methods Mol. Biol.* **1279,** 45–65 (2015).
61. Wu, H. *et al.* Metformin alters the gut microbiome of individuals with treatment-naive type 2 diabetes, contributing to the therapeutic effects of the drug. *Nat. Med.* **23,** 850–858 (2017).
62. Steinbeck, C. *et al.* Recent developments of the chemistry development kit (CDK) - an open-source java library for chemo- and bioinformatics. *Curr. Pharm. Des.* **12,** 2111–2120 (2006).
63. Kim, S. *et al.* PubChem substance and compound databases. *Nucleic Acids Res.* **44,** D1202–D1213 (2016).

© 2018 Macmillan Publishers Limited, part of Springer Nature. All rights reserved.

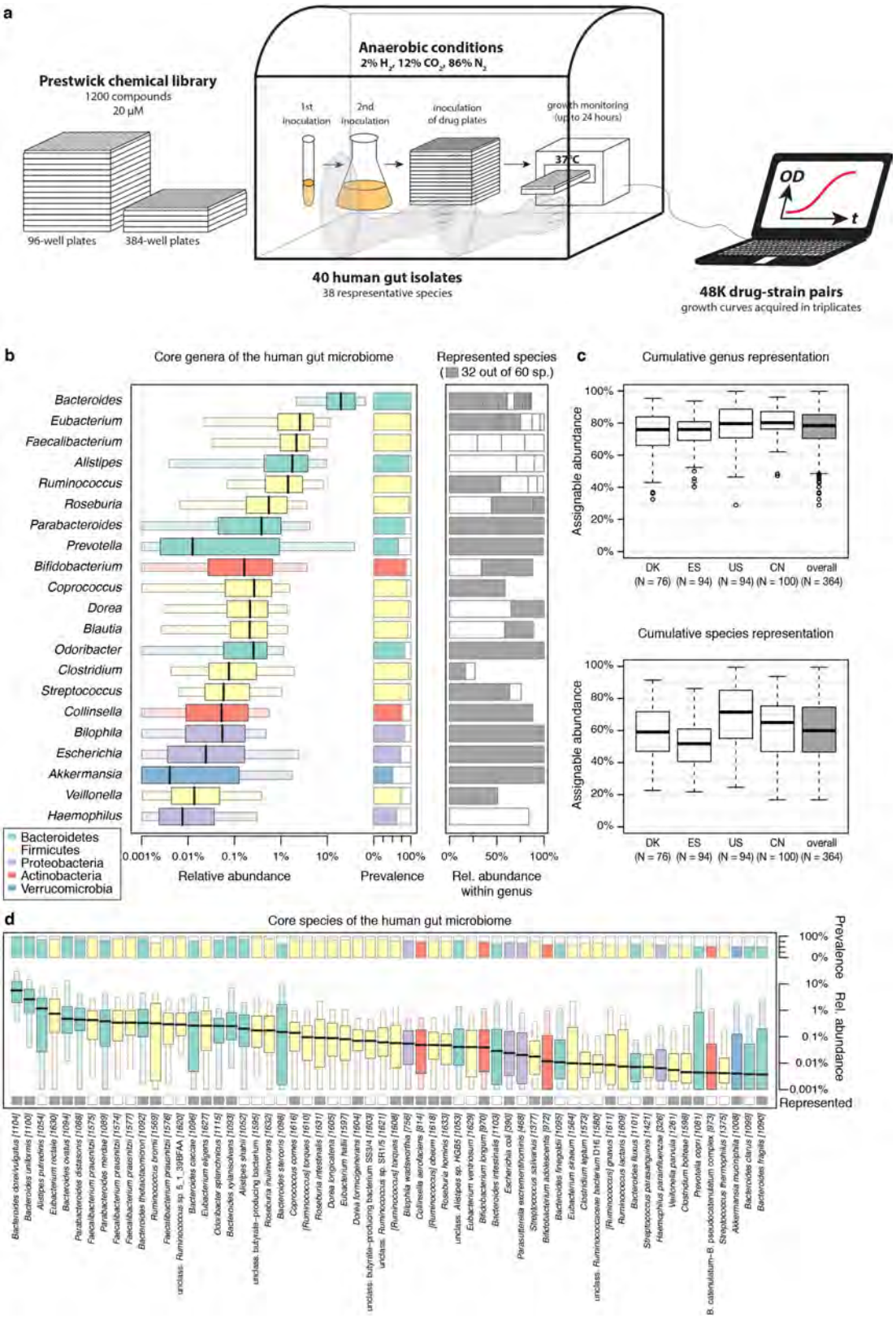

Extended Data Figure 1 | See next page for caption.

© 2018 Macmillan Publishers Limited, part of Springer Nature. All rights reserved.

Extended Data Figure 1 | Screen set-up and species selection. a, Drugs from the Prestwick Chemical Library (arranged in either 96- or 384-well format) were diluted in growth medium (usually mGAM) and pre-reduced in a Coy anaerobic chamber before inoculation with one of forty different human gut microbes. Bacterial growth was monitored for 16–24 h at 37 °C. Growth curves were acquired at least in triplicate for each drug–microbe interaction (see Methods). **b**, Species with a minimum relative abundance of 1% in at least one sample and a prevalence of 50% across samples (the latter estimated by rarefying to 10,000 reads mapping to taxonomic markers) were included in the set of core species. Boxplots show relative abundances of core species grouped by genus (according to NCBI taxonomy) and coloured by phylum (see key). The inner box indicates the IQR, with the median as black vertical line; the outer bars extend to the 5th and 95th percentiles; circles, outliers. To the right of the boxplots, prevalence is depicted by bars, and next to this the species diversity is shown; grey boxes indicate species represented in the screen with box widths corresponding to mean relative abundance within the genus. **c**, Relative abundance of genera of which at least one species was represented in the screen cumulates to 78% of the assignable fraction of reads (median across all samples, upper panel); first four boxplots show abundance within each study identified by country codes underneath (DK: Denmark; ES: Spain; US: United States; CN: China) [43–46]. When directly cumulating the relative abundance of represented species the corresponding median is 60% (lower panel). Boxes span the IQR and whiskers extend to the most extreme data points up to a maximum of 1.5 times the IQR. **d**, Core species are shown in the order of their median abundances across all samples. Relative abundance boxplots and prevalence bars are defined as in **b** and grey boxes underneath indicate species screened in this study. Numbers in brackets correspond to specI cluster identifiers (version 1)[47].

© 2018 Macmillan Publishers Limited, part of Springer Nature. All rights reserved.

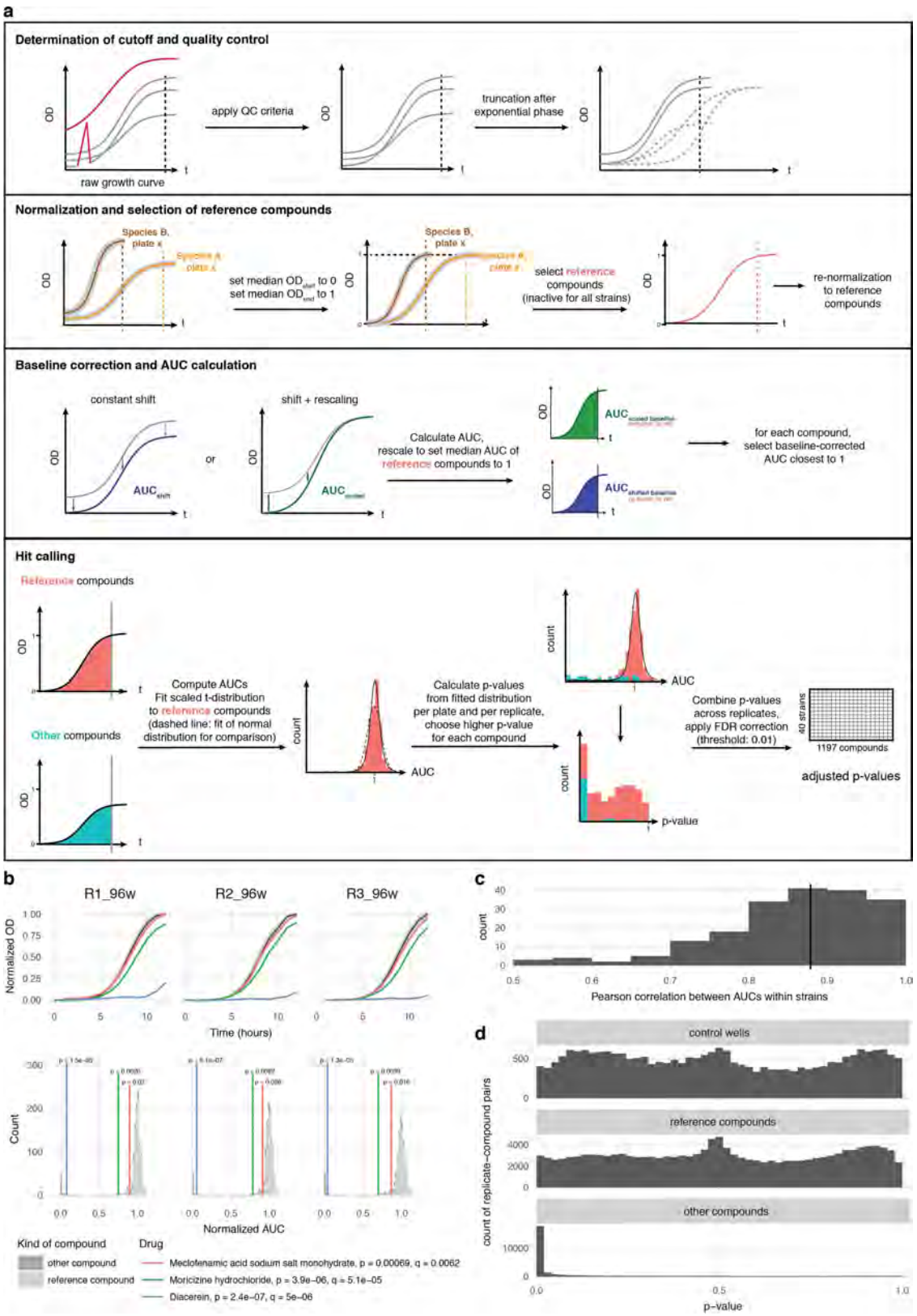

Extended Data Figure 2 | See next page for caption.

© 2018 Macmillan Publishers Limited, part of Springer Nature. All rights reserved.

Extended Data Figure 2 | Data analysis pipeline for identifying compounds with anticommensal activity. a, Schematic overview of the data analysis pipeline. All steps (determination of time cutoff and removal of noisy points; normalization and selection of reference compounds; baseline correction and AUC calculation; and hit calling) are explained in detail in the Methods. On the first panel, dashed curves in the righthand plot depict the three possible effects that a drug can have on the growth of a microbe: increase the lag phase, decrease the growth rate or the stationary phase plateau. All effects are captured by cutting off the growth curves upon transition to stationary phase for most compounds (most drugs do not affect growth). On second panel, median growth rates for two drugs on same plate are depicted and normalized, whereas baseline correction (third panel) is applied at the individual wells. **b**, Growth curves (top, normalized OD) of *Bacteroides ovatus* in three exemplary drug cases for the three biological replicates (meclofenamic acid (red), moricizine (green) and diacerein (blue)). Light and dark grey shades represent the 50% and 90% confidence intervals for normal growth, respectively. Bottom, normalized AUC histograms for all drugs in the three biological replicates for *B. ovatus*. Meclofenamic acid is just below the hit threshold, moricizine is a hit with partial but strong growth inhibition, and diacerein almost completely inhibits the growth of *B. ovatus*. **c**, For most species, correlation between replicates is very high (median: 0.88). **d**, For both controls and reference compounds, *P* values were approximately uniformly distributed. Determining the background distribution of uninhibited growth using reference compounds is validated by their very similar behaviour with control wells. Other drugs (that is, drugs not used as reference compounds) show clear enrichment of low *P* values.

© 2018 Macmillan Publishers Limited, part of Springer Nature. All rights reserved.

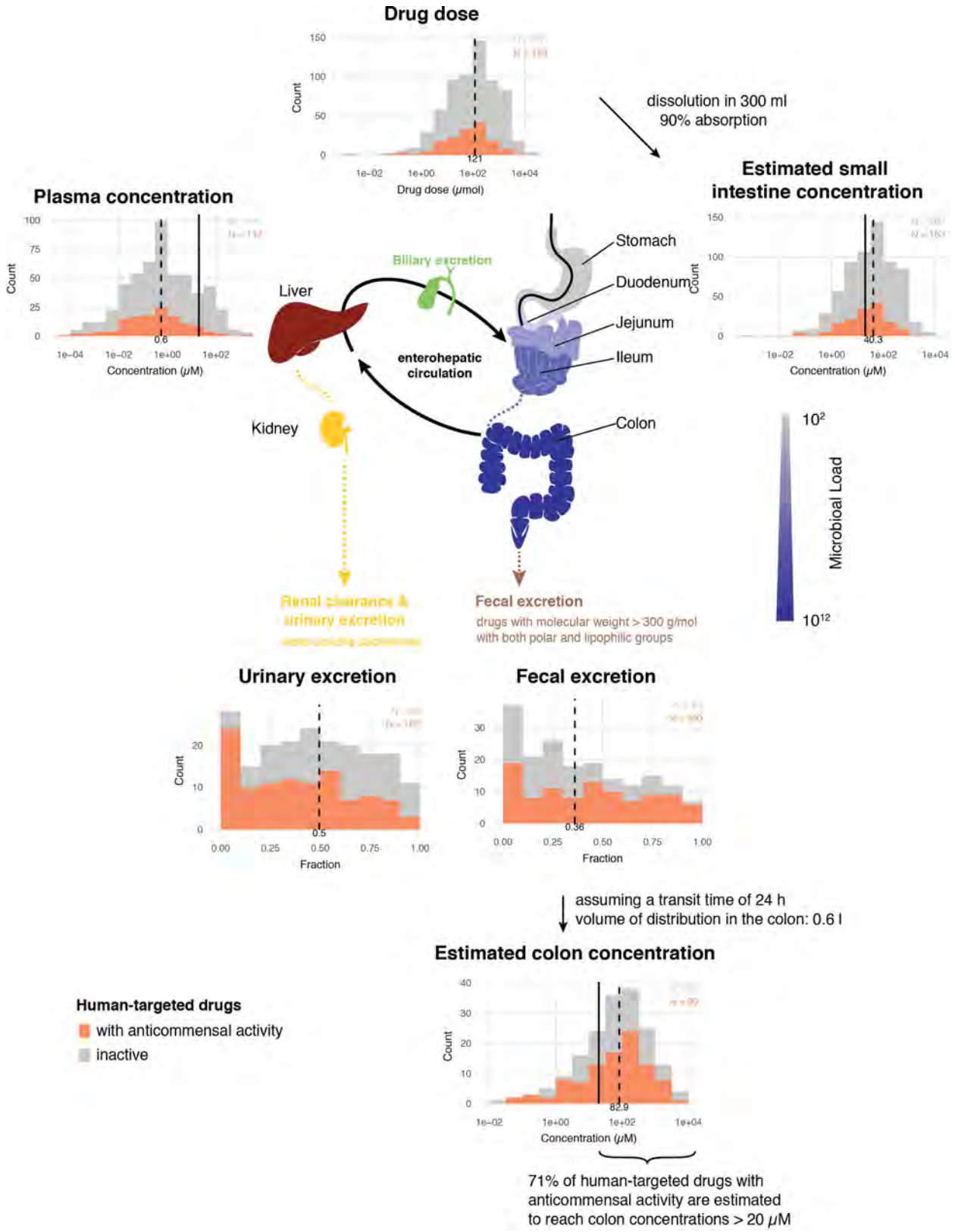

Extended Data Figure 3 | See next page for caption.

© 2018 Macmillan Publishers Limited, part of Springer Nature. All rights reserved.

Extended Data Figure 3 | Anticommensal activity relative to compound- and compartment-specific drug concentrations. We made a simplified pharmacokinetic estimation of small intestine and colon concentrations by assuming that one dose of an orally administered drug (extracted from Drugs@FDA and Daily Defined Dose (DDD) of the ATC) reaches the intestine and is dissolved or absorbed similarly to the well-absorbed drug posaconazole[19] (Supplementary Table 1). After absorption into the liver via the portal circulation, the drug enters circulation through the hepatic veins and reaches its characteristic plasma concentration. The two main routes of drug elimination are either secretion via kidneys and urine or secretion into the intestine via the biliary duct. In the intestine, drugs can be reabsorbed in a circuit called the enterohepatic cycle or excreted in stools. Compounds that are either poorly absorbed in the small intestine or secreted by bile reach the large intestine. Considering the measured excreted fraction of the drug in faeces (both changed and unchanged compound, as we do not know whether drug is metabolized in liver or gut), and assuming a large intestinal transit time of 24 h[55] and a volume of distribution in the colon of 0.6 l[56], we estimated the colon concentrations of the human-targeted drugs in our screen (Supplementary Table 1). Histograms for drug dose, plasma concentration, estimated small intestine concentration, urinary and fecal excretion and estimated colon concentration depict the respective distributions for human-targeted drugs, colour coded according to their anticommensal behaviour in our screen. Dashed lines indicate medians and vertical lines highlight the drug concentration used in our screen (20 μM). Interactions between drugs and microbiota are possible throughout the entire gastrointestinal tract, with microbial load having a gradient-like distribution (ileum and colon containing the largest numbers); this can be disturbed during disease[18]. In addition, drugs can be modified at several stages: by host digestive and intestinal epithelial enzymes, by phase I and phase II metabolism in the liver and by microbial enzymes. Some of these processes neutralize each other, resulting in reconversion into the original compound.

© 2018 Macmillan Publishers Limited, part of Springer Nature. All rights reserved.

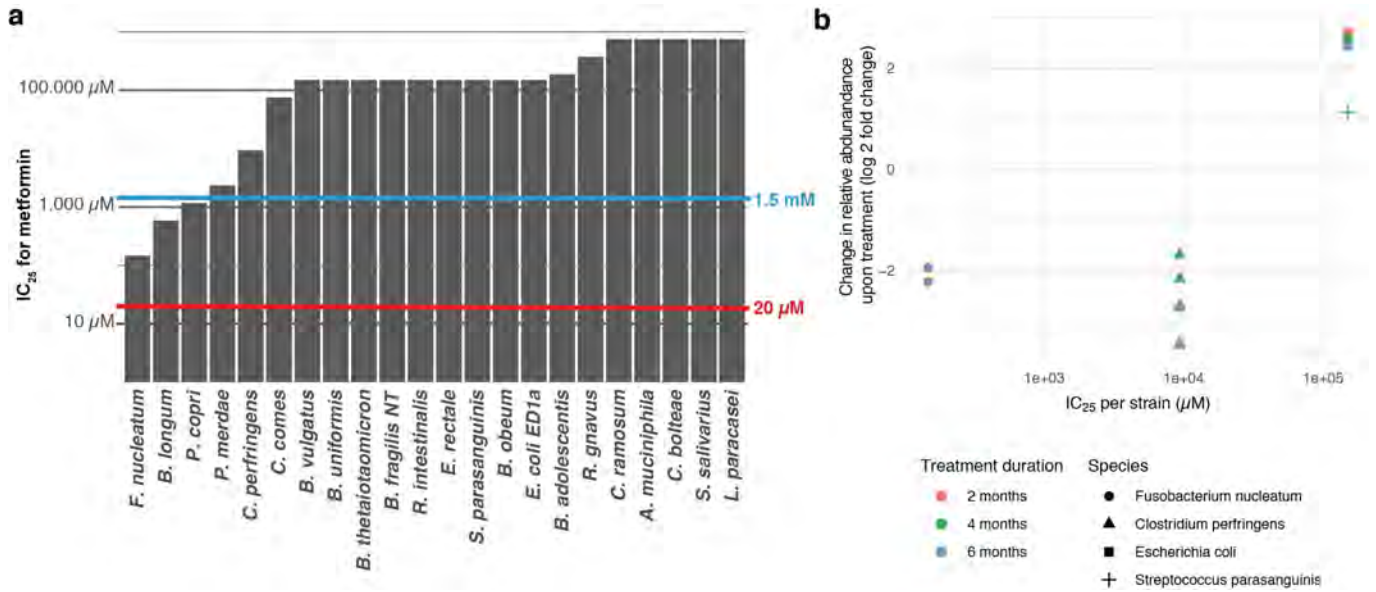

Extended Data Figure 4 | Effects of metformin in gut microbiota *in vivo* correlate with its *in vitro* activity. a, IC_{25}s of the antidiabetic drug metformin for a selection of 22 strains. Metformin did not inhibit any species in our screen as the concentration used, 20 μM (red line), is below the IC_{25} of all strains. However, at its estimated small intestinal and colon concentration of 1.5 mM (blue line), metformin would inhibit 3 of 22 tested strains. This exemplifies that more human-targeted drugs would interfere with bacterial growth if doses were to be increased towards drug- and body-site-specific concentrations. **b**, IC_{25}s of metformin correlate well with its observed effects in humans[61], based on the four species that overlapped between the two studies. Significant treatment effects on the species level were mapped to our set of strains for which we had determined IC_{25}s.

© 2018 Macmillan Publishers Limited, part of Springer Nature. All rights reserved.

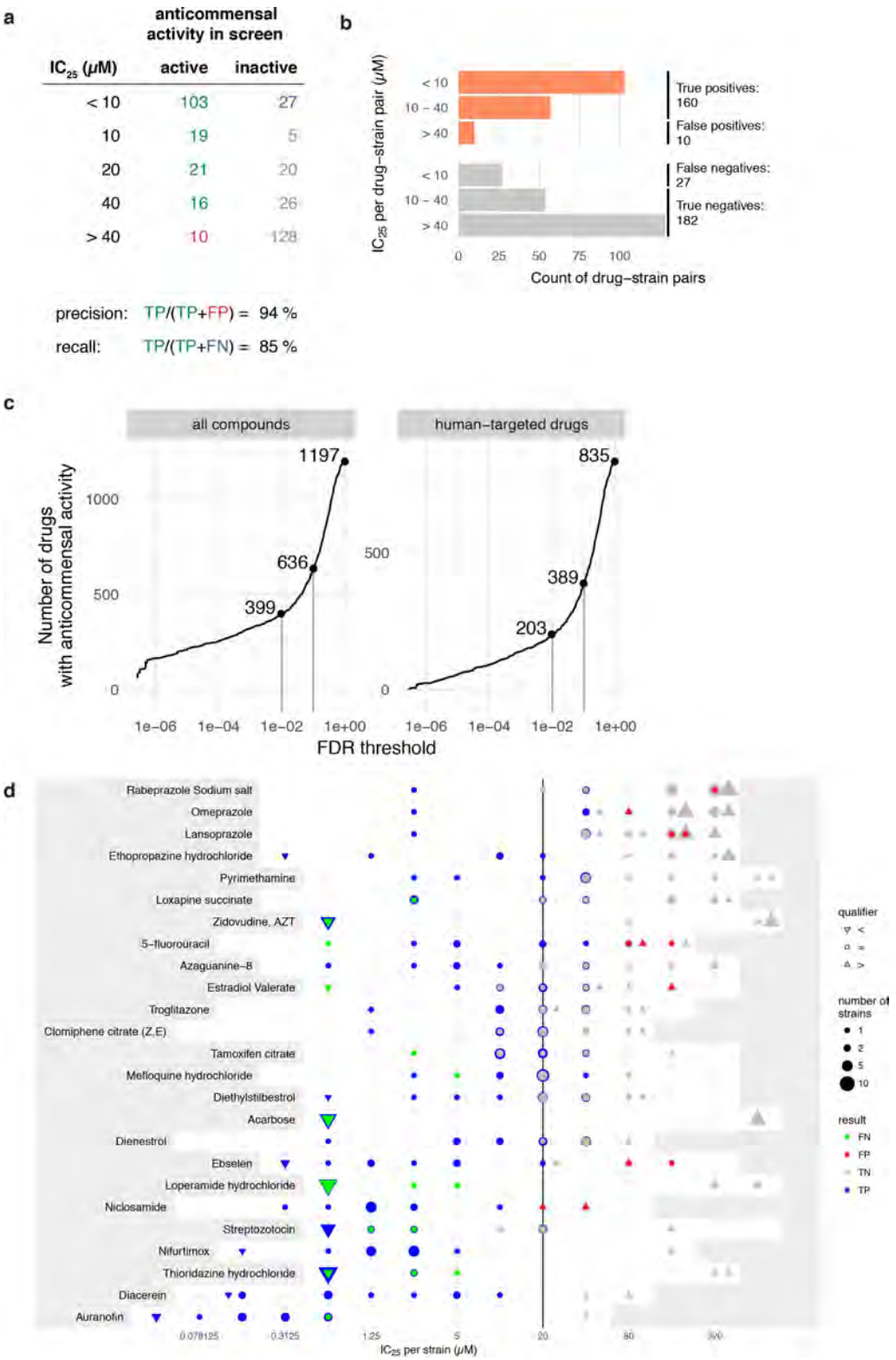

Extended Data Figure 5 | Validation of the screen and conservative hit-calling. a, **b**, Validation of our screen by IC_{25} determination for 25 selected drugs in a subset of up to 27 strains reveals high precision (94%) and recall (85%). We considered IC_{25} as the lowest concentration that reduces growth by at least 25% (see Methods). Breakdown into active and inactive compounds for drugs concentrations at the 20 μM concentration, used in our screen. True positives (TP), green; false positives (FP), red; true negatives (TN), grey; false negatives (FN), blue. **c**, Number of drugs with anticommensal activity versus the applied FDR threshold for all compounds (left) and human-targeted drugs (right). Increasing the FDR threshold from 0.01 to 0.1 (vertical grey lines) would nearly double the fraction of drugs that affect human gut microbes. **d**, IC_{25}s of 25 drugs in up to 27 individual strains (see also **a**, **b**). The white area indicates the drug concentration range tested for each drug. Symbol sizes depict the number of strains with a particular IC_{25}, symbol colours indicate categorization into false negative, false positive, true negative and true positive, and symbol shapes qualify whether actual IC_{25}s were determined or IC_{25} was deemed to be higher or lower than the highest or lowest concentration tested, respectively. Vertical line indicates the drug concentration used in screen (20 μM). IC_{25}s for all drug–strain pairs are listed in Supplementary Table 4. Particular drugs were responsible for false negatives in our screen (acarbose, loperamide, thioridazine), presumably owing to drug decay.

© 2018 Macmillan Publishers Limited, part of Springer Nature. All rights reserved.

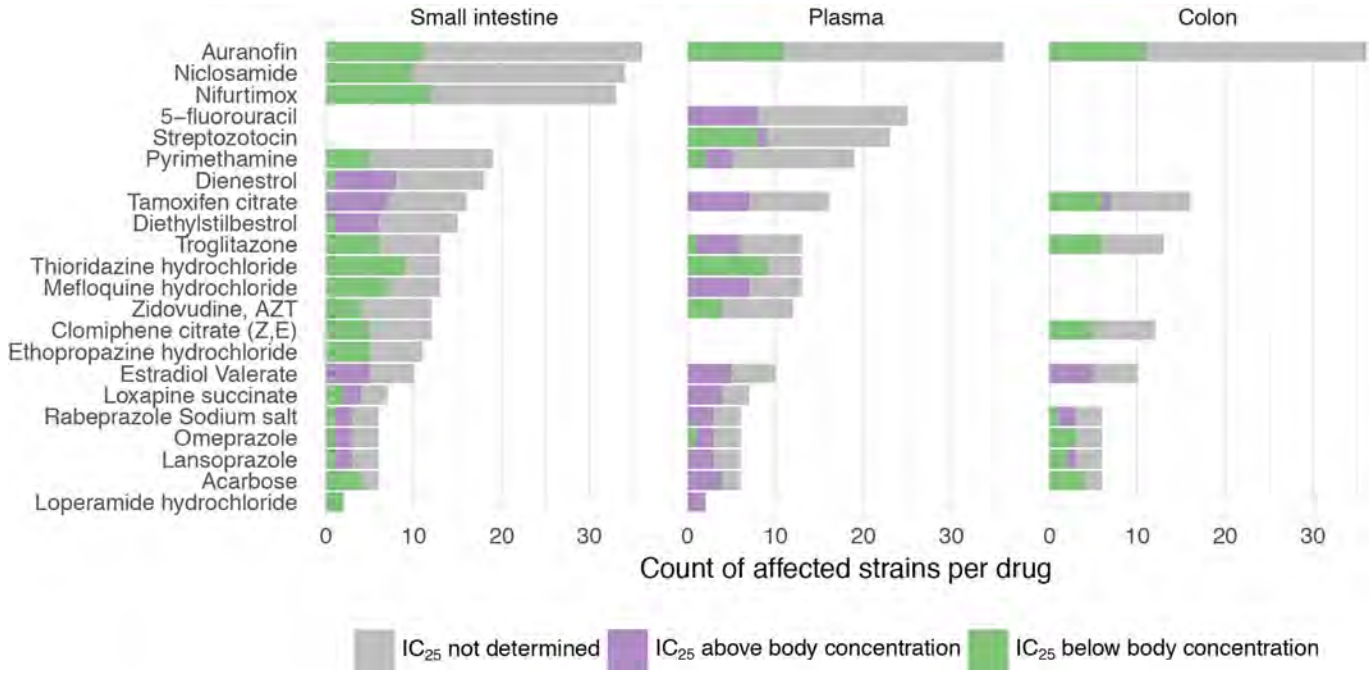

Extended Data Figure 6 | IC_{25} relation to drug concentrations in human body. For drug–strain pairs with measured IC_{25}s (see also Extended Data Fig. 5), we compared IC_{25}s with plasma and estimated small intestine and colon concentrations by plotting the number of strains that are affected in relation to whether they are above or below relevant body concentrations (colour code). With the exception of oestradiol valerate and 5-FU (only plasma concentrations available), all other drugs with available body concentrations reach concentrations high enough in the body to reach their IC_{25} for at least one gut microbial species (out of up to 27 species tested for IC_{25}s).

© 2018 Macmillan Publishers Limited, part of Springer Nature. All rights reserved.

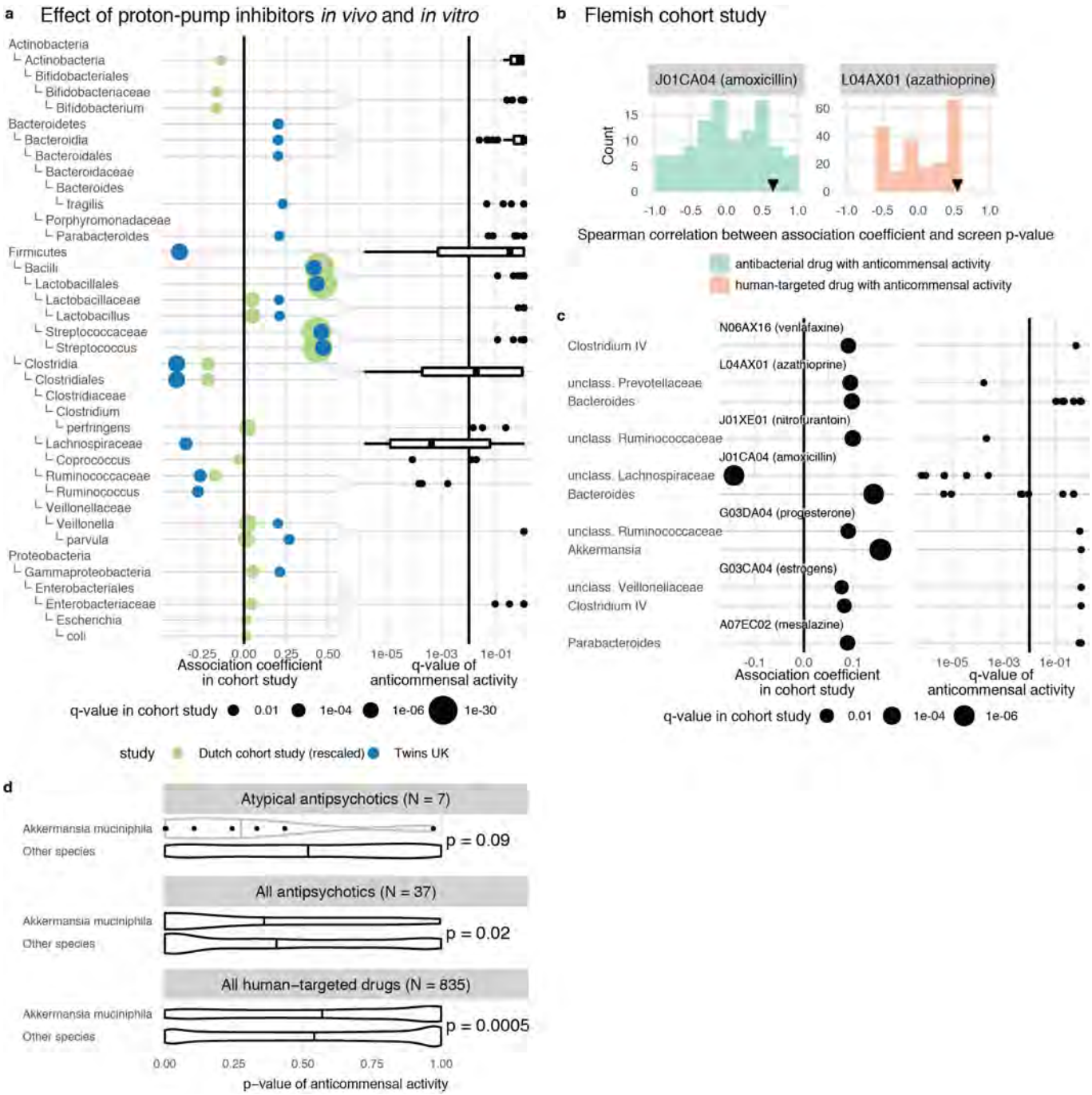

Extended Data Figure 7 | Concordance of drug *in vitro* species susceptibilities and drug-mediated shifts in microbiome composition of patients. a, Association coefficients between PPI usage and relative taxonomical abundance in faecal microbiomes of PPI users from two studies (twins, UK cohort, green[4]; three independent cohorts from the Netherlands[3], blue) (left) are compared to *in vitro* growth inhibition of isolates with same taxonomic rank in the presence of PPIs (omeprazole, lansoprazole and rabeprazole) as assessed by FDR-adjusted *P* values (*q* values) in our screen (right). Point size in the left panel corresponds to the *q* value as reported in the original study. Taxa that were reduced in patients (negative association coefficient, left of vertical black line) were mostly inhibited by PPIs in our screen (*q* value below 0.01, left of vertical black line), whereas enriched taxa were insensitive to PPIs. Box plots show: centre line, median; box limits, upper and lower quartiles; whiskers, 1.5× IQR; points, outliers. For fewer than 10 data points, all points are shown individually. **b**, Spearman correlation coefficients between association coefficients of faecal microbiome composition after consumption of amoxicillin or azathioprine[7] and the screen *P* values. The histogram represents the background distribution of correlations between the *in vitro* data for all human-targeted drugs and the *in vivo* response to these drugs; correlations with amoxicillin or azathioprine are highlighted by triangles **c**, Comparisons between association coefficients and drugs from different therapeutic classes as assessed by Falony *et al.*[7] and our *in vitro* data. **d**, A study of a cohort of patients with bipolar disease[6] reported a significant decrease in abundance of *Akkermansia* upon treatment with atypical antipsychotics (AAP). When we compared distributions of adjusted *P* values from our screen for different strains, *Akkermansia muciniphila* was significantly more sensitive than all other strains to antipsychotics in general and APP in particular ($P = 0.02$ and $P = 0.09$, two-sided Wilcoxon rank sum test). By contrast, *A. muciniphila* is relatively more resistant than other strains across all human-targeted drugs ($P = 0.0005$, two-sided Wilcoxon rank sum test). Violin plot shows estimated density of points with the estimated median as vertical bar. For fewer than 10 data points, all points are also shown individually.

© 2018 Macmillan Publishers Limited, part of Springer Nature. All rights reserved.

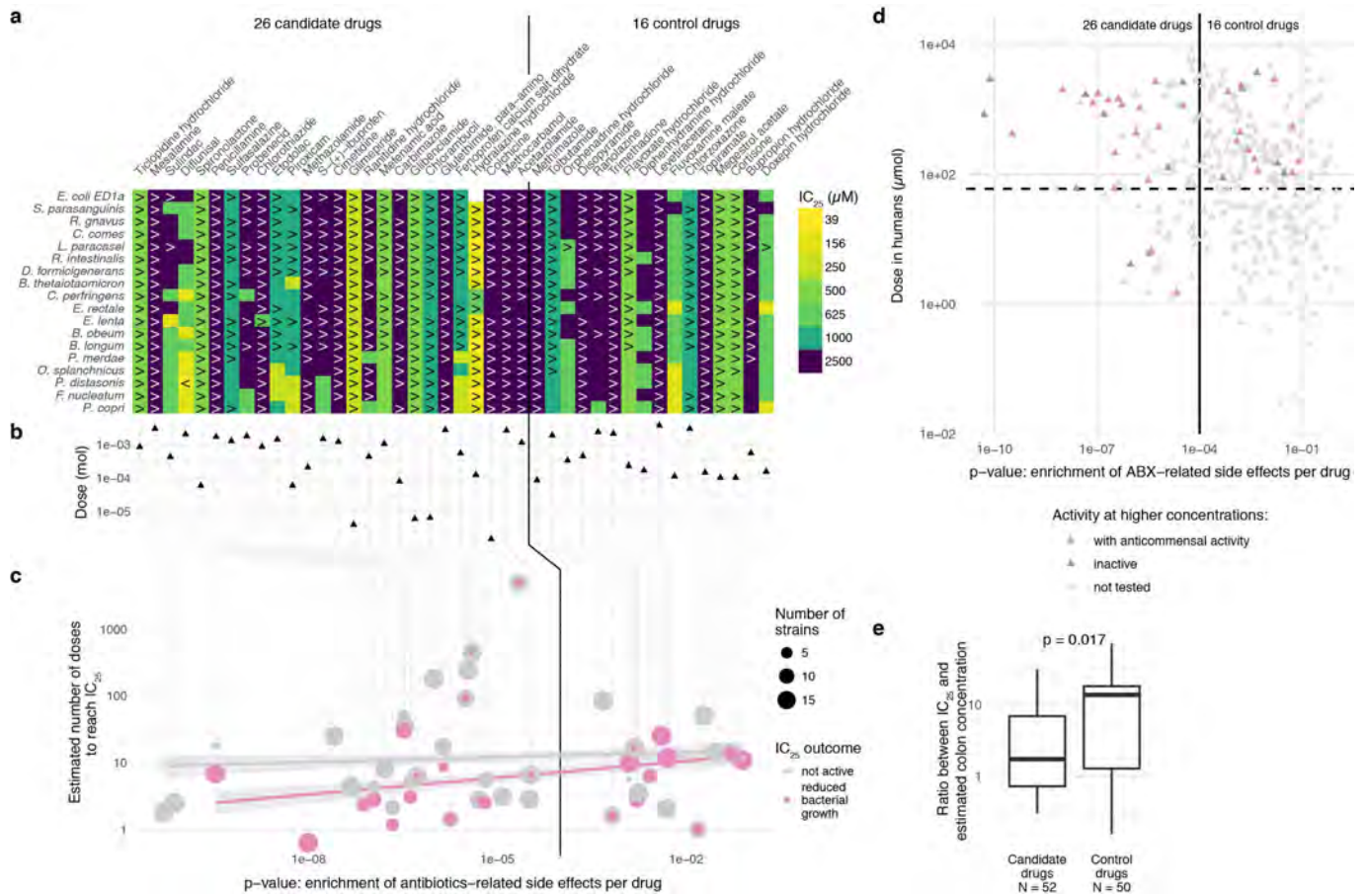

Extended Data Figure 8 | Evaluation of anticommensal activity predictions based on side-effects. a, IC_{25}s of 26 candidate compounds (P value for enrichment of antibiotic-related side effects $<1\times10^{-4}$, using a one-sided Fisher's exact test) and 16 control compounds (see also **d** of this Figure) were determined for 18 representative strains; results are depicted as an IC_{25} heatmap. Drugs are ordered according to their similarity in side effects to antibiotics from left to right (for antibiotic-related side effects see Supplementary Table 5). Qualifiers indicate whether IC_{25}s are higher or lower than the indicated concentration; if no symbol, the box depicts the exact IC_{25}. If highest tested concentrations did not reduce growth of any of the tested strains, the compound was classified as inactive (for example, Topiramate). **b**, Dose of the tested compounds according to the Defined Daily Dose and Drugs@FDA databases (see also Supplementary Table 1). **c**, Based on a compound's recommended dose and its median IC_{25} for different bacterial strains, we estimated the number of doses need to reach this IC_{25}. This number was plotted against the drug's P value for enrichment of antibiotic-related side effects. For direct comparison between the two groups, see Fig. 3c. Circles in magenta depict drug–strain pairs for which growth was reduced, showing a clear correlation between P values and the estimated number of doses (magenta line). To rule out the possibility that the tested concentration range is causing this correlation, we also depict the estimated number of doses corresponding to the highest tested concentration (grey line), which exhibits no clear dependency between P value and number of doses. A vertical line across all panels connects all parameters attributable to a particular drug. **d**, Recommended single drug doses of human-targeted drugs with no anticommensal activity in our screen plotted against enrichment in antibiotic-related side effects ($n=339$). Candidate and control drugs selection for testing for anticommensal activity at higher concentrations were selected on the basis of similarity to antibiotic-related side effects (vertical black line depicts prediction threshold) and aiming at drugs used at higher doses than concentration in our screen (horizontal dashed line). Purple and dark grey triangles indicate hits and non-hits from this validation effort, respectively. **e**, Ratios between IC_{25} and estimated colon concentrations are significantly lower ($P=0.017$, two-sided Wilcoxon rank sum test) for candidate drugs than for control drugs. For candidate drugs, 16 of 52 (31%) IC_{25}s were below the estimated colon concentrations while for control drugs this fraction was only 5 of 50 (10%). Box plots show: centre line, median; box limits, upper and lower quartiles; whiskers, 1.5× IQR; points, outliers.

© 2018 Macmillan Publishers Limited, part of Springer Nature. All rights reserved.

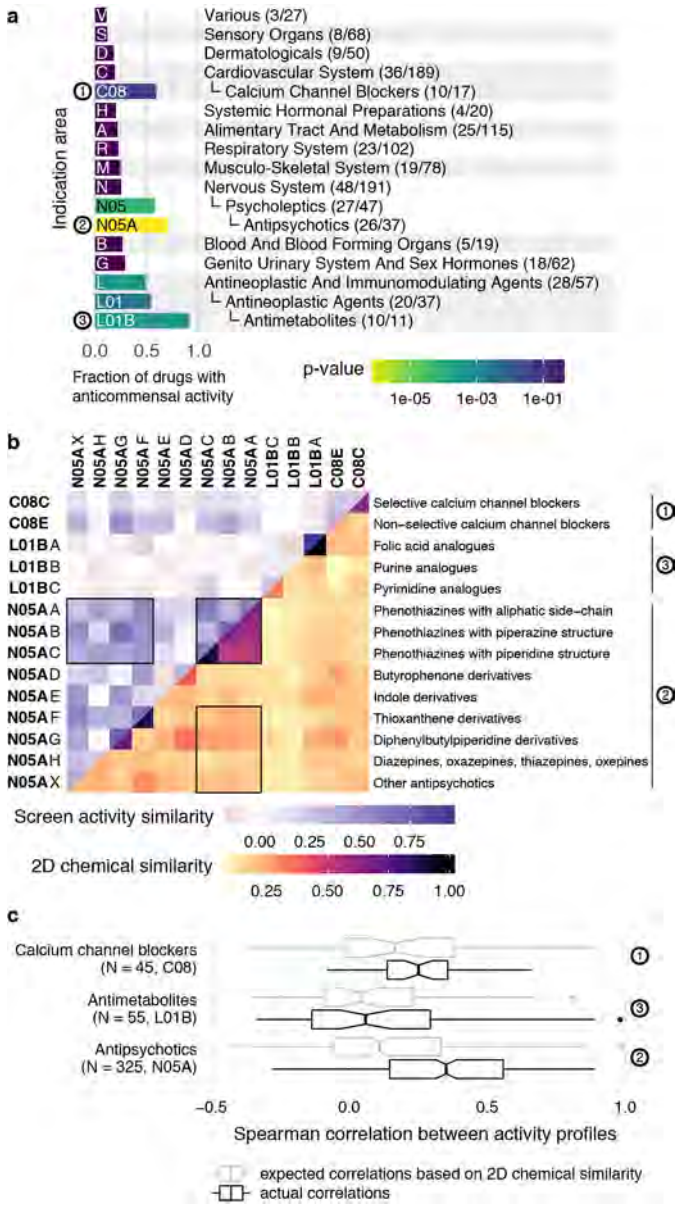

Extended Data Figure 9 | Drug therapeutic classes with anticommensal activity. a, Fraction of drugs with anticommensal activity by ATC indication area (bars). All first-level indication areas and significantly enriched lower levels are shown (see also Extended Data Fig. 10). Significance (*P* value, one-sided Fischer's exact test) is controlled for multiple hypothesis testing (Benjamini–Hochberg) independently at each ATC hierarchy level. **b**, Heat map of anticommensal activity and chemical similarities of human-targeted drugs within the three significantly ATC indication levels from **a** (indicated by circled numbers). Colours represent the median of drug pairwise Spearman correlations within and between subgroups depicted, calculated from the growth profiles of the 40 strains in each drug (*P* values) or their chemical similarity (Tanimoto scores[62]). Examples of structurally similar (phenothiazines; N05AA-AC) and diverse (N05AF-AX) antipsychotics that elicit similar responses in our screen are marked. **c**, Antipsychotics exhibit higher similarity in gut microbes they target than that expected on the basis of their structural similarity ($P = 2 \times 10^{-19}$ estimated from random permutations; other classes depicted show no significance difference). Box plots show: centre line, median; box limits, upper and lower quartiles; whiskers, 1.5× IQR; points, outliers. Notches correspond roughly to a 95% confidence interval for comparing medians.

© 2018 Macmillan Publishers Limited, part of Springer Nature. All rights reserved.

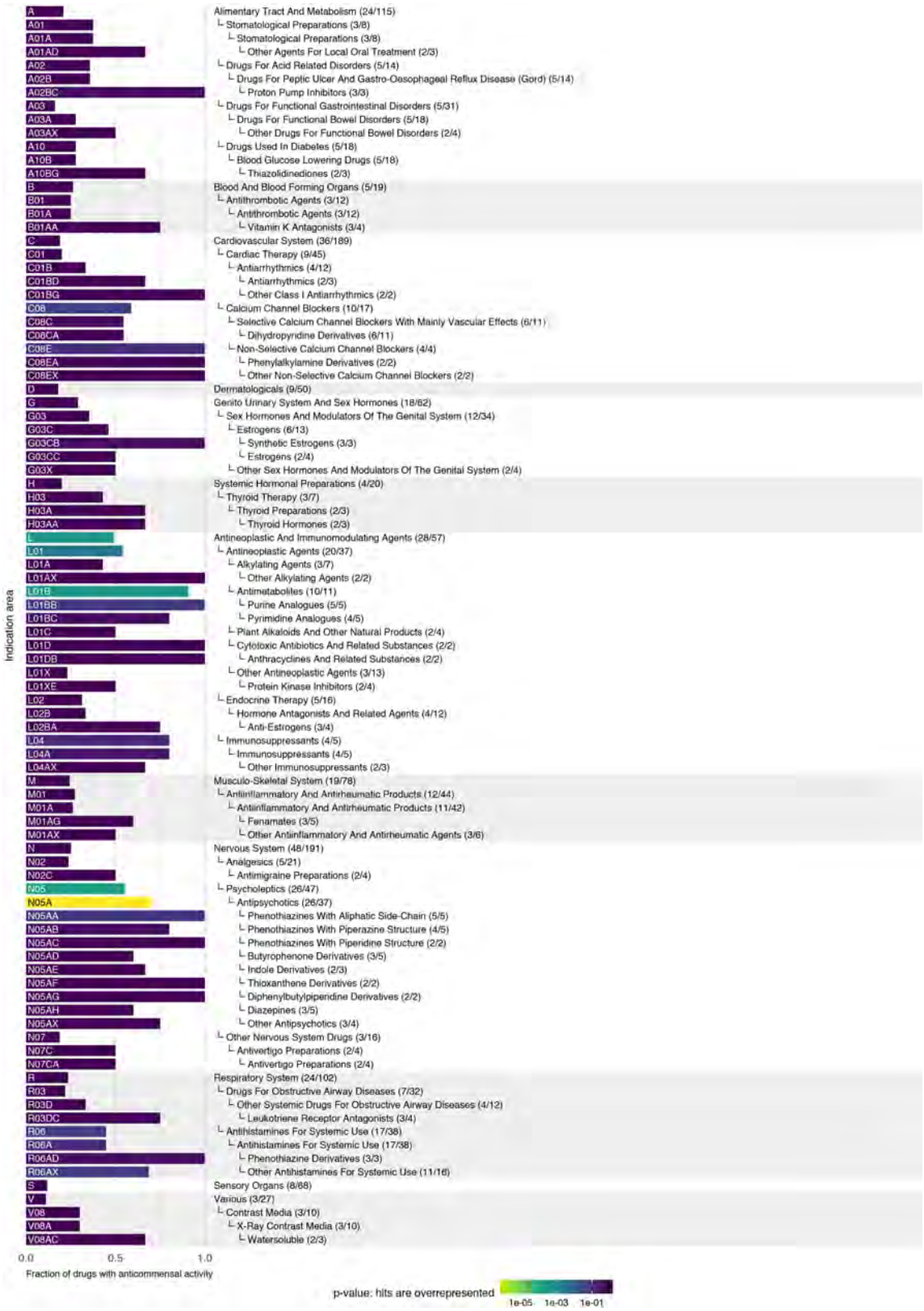

Extended Data Figure 10 | Drugs with anticommensal activity for all hierarchy levels of the ATC classification system. Fraction of drugs with anticommensal activity for all indication areas of the ATC classification scheme with a high fraction of active compounds. Shown are indication areas that contain at least two active compounds and a fraction of at least 50% active compounds, their parent terms and all top-level indication areas. Significance (*P* value, one-sided Fischer's exact test) is indicated by the bar colour and corrected for multiple hypothesis testing (Benjamini–Hochberg) independently at each hierarchy level of the ATC. Many smaller classes, including PPIs (A02BC), non-selective calcium channel blockers (C08E), synthetic oestrogens (G03CB), leukotriene receptor antagonists (R03DC) and phenothiazine and other antihistamines (R06AD and R06AX) are enriched, but owing to multiple testing and the small numbers of drugs tested in each group, they do not reach a significant *P* value.

© 2018 Macmillan Publishers Limited, part of Springer Nature. All rights reserved.

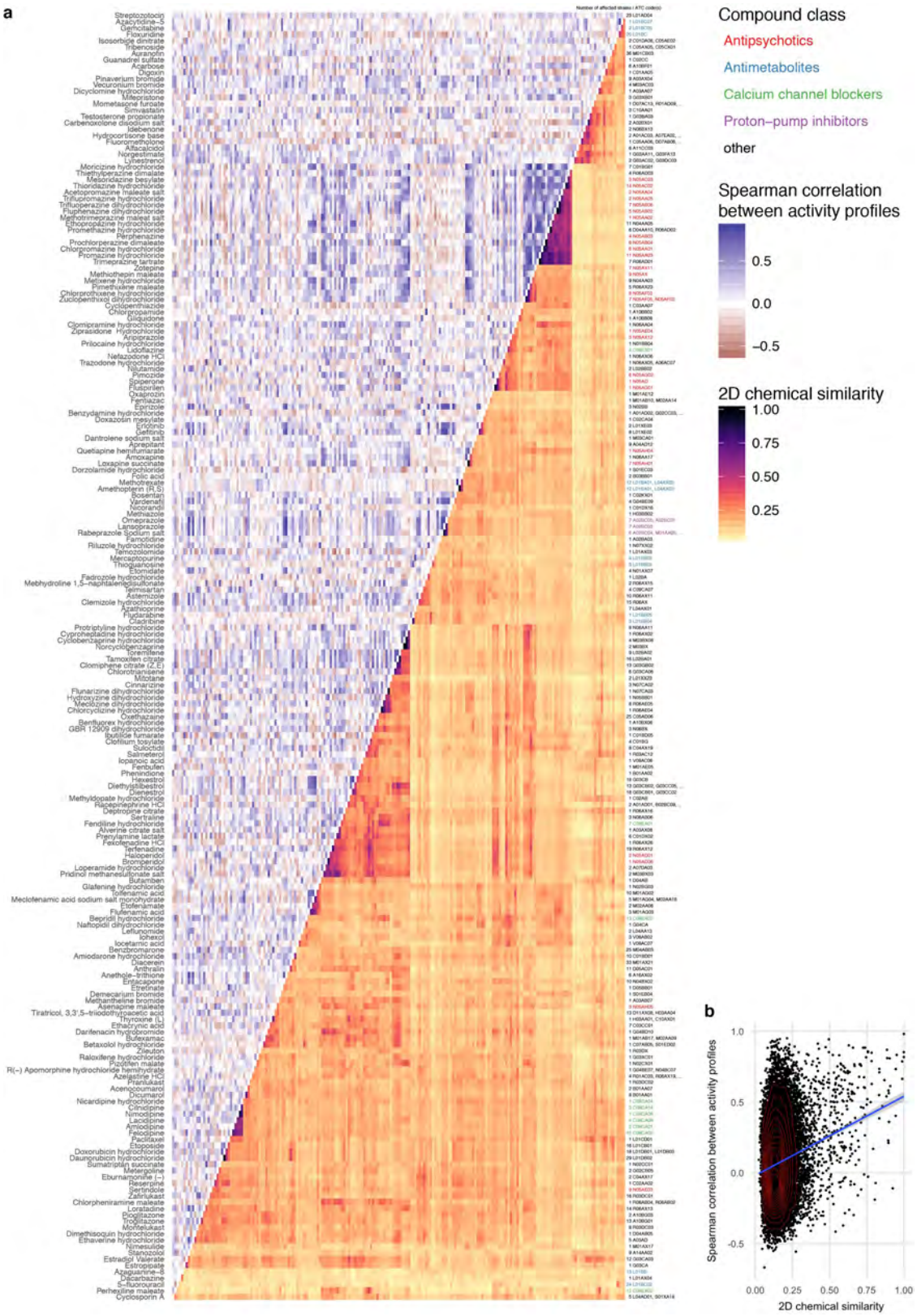

Extended Data Figure 11 | Comparing chemical similarity of drugs and similarity of hit profiles across gut microbes. a, Heat map of anticommensal activity and chemical similarities for all active human-targeted drugs in our screen. Drugs are clustered according to chemical similarity. Colours represent the median of drug pairwise Spearman correlations within and between subgroups depicted, calculated from the growth profiles of the 40 strains in each drug (*P* values) or their chemical similarity (Tanimoto scores[62]). Several prominent groups are colour coded. Only drugs of some classes both share chemical similarity and have similar effects on the 40 strains—for example, phenothiazine antipsychotics and antihistamines (N05A and R06AD), structurally similar dibenzothiazepines and dibenzoxazepines for antipsychotics and antidepressants (N05AH and N06AA), PPIs (A02BC), anti-oestrogens (L02BA), synthetic oestrogens (G03CB) and anti-inflammatory fenamates (M01AG and M02AA06). **b**, A mild correlation exists between chemical similarity (Tanimoto scores) and anticommensal activity similarity (drug pairwise Spearman correlations): $r_s = 0.12$ (*P* value of Spearman's test $< 2 \times 10^{-16}$).

© 2018 Macmillan Publishers Limited, part of Springer Nature. All rights reserved.

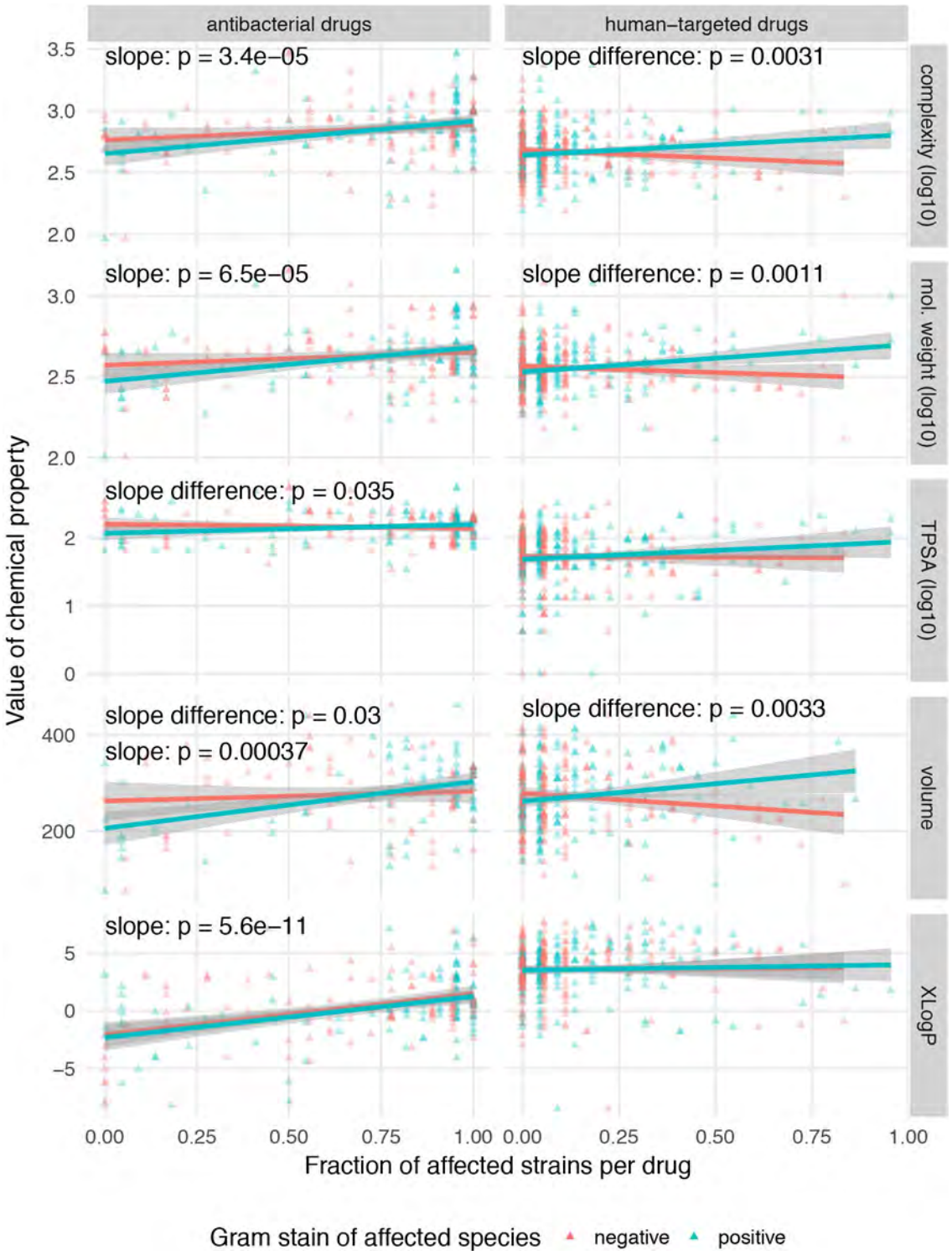

Extended Data Figure 12 | More complex, bulkier and heavier human-targeted drugs are more effective against Gram-positive bacteria. Fraction of inhibited Gram-positive (blue, $n = 22$) or Gram-negative (red, $n = 18$) strains per drug plotted against different chemical properties of the drugs. Chemical properties, such as complexity (based on atom types, symmetry, computed using the Bertz/Hendrickson/Ihlenfeldt formula), molecular weight, TPSA (an estimate of the area, in $Å^2$), volume (in $Å^3$) and XLogP (distribution coefficient that is a measure of differential solubility in octanol and water) were obtained from PubChem[63]. For each chemical property, we used a type II ANOVA to test for linear dependency between the fraction of affected species and the chemical property (slope). Additionally, we tested whether this dependency depended on the Gram stain (slope difference). It is possible that there is no significant slope without considering Gram stain, but that there is a significant difference between the slopes for the two Gram stains. Lines show a linear fit to the data, with 95% confidence intervals as shaded area.

© 2018 Macmillan Publishers Limited, part of Springer Nature. All rights reserved.